NASA-CR-172348

NASA Contractor Report 172348

NASA-CR-172348
19840018305

Advanced Laser Stratospheric Monitoring Systems Analyses

Jack C. Larsen

Systems and Applied Sciences Corporation
17 Research Drive
Hampton, VA 23666

Contract NAS1-15806
June 29, 1984

LIBRARY COPY

1984

LANGLEY RESEARCH CENTER
LIBRARY, NASA
HAMPTON, VIRGINIA

NASA
National Aeronautics and Space Administration
Langley Research Center
Hampton, Virginia 23665

TABLE OF CONTENTS

N84-26373#

SUMMARY

This report describes the software support supplied by Systems and Applied Sciences Corporation for the study of Advanced Laser Stratospheric Monitoring Systems Analyses under contract No. NAS1-15806. This report discusses improvements to the Langley spectroscopic data base, development of LHS instrument control software and data analyses and validation software. The effect of diurnal variations on the retrieved concentrations of NO, NO_2 and ClO from a space and balloon borne measurement platform are discussed along with the selection of optimum IF channels for sensing stratospheric species from space.

SECTION 1 - INTRODUCTION

SASC efforts during this contract were directed primarily toward support of the Laser Heterodyne Spectrometer (LHS).

LHS is based on the optical heterodyne concept. Infrared radiation emitted by the sun and attenuated by atmospheric constituents photomixes with radiation from the tunable diode laser (TDL) local oscillator (LO) to produce an upper and lower side-band at radio frequencies. The frequency pass band of the detector determines the upper limit of the radio frequencies. The radio frequency band pass is further divided up into channels with each channel containing contributions from the upper and lower side-bands. The spectral resolution of the instrument will be determined by the channel band widths and is typically less than .01 cm^{-1}. The use of a tunable diode laser can produce a signal enhancement over that of a fixed frequency laser when tuned to the peak of an absorption line. The high spectral resolution coupled with the LO tunability offers a great advantage to distinguish discrete absorption lines from interferring lines when tenuous trace gases in the atmosphere are to be measured. The final output of the instrument will be a voltage signal proportional to the input signal radiance.

The mathematical simulations presented in this report are based on three computer codes used to model the LHS measurement scenario. The atmospheric model is a line by line radiative transfer code developed by Clayton Bair at NASA/Langley that calculates transmission through the atmosphere for the

occultation geometry over narrow spectral regions. The instrument model converts the solar irradiance to digitized voltages assuming realistic instrument parameters. The instrument model provides a measure of the RMS noise voltage. The retrieval algorithm converts the vertical profiles of digitized voltages to vertical concentration profiles of the target gases. The instrument configuration and mathematical model of the instrument are further explained in Appendix A. Appendix B contains a description of the retrieval algorithm.

Since LHS is a high resolution instrument the ability to perform measurement feasibility studies or to reduce measurement data depends greatly on the availability of accurate line absorption parameters. The IF channels may be configured many different ways with each configuration effecting the random noise characteristics of the retrievals. Radical species, such as NO, NO_2 and ClO, that have strong diurnal concentration variations will no longer be symmetric about the tangent point and will produce constant bias type of errors in the retrieved concentration. Under this contract studies were carried out to determine the optimum IF channels for several different trace species. The effect of diurnal variations on the retrieval of several trace species was studied. The spectroscopic data base was improved and software was developed to control the LHS instrument subsystems and to analyze and validate LHS measurement data. Work completed under this contract has supported several publications (refs. 1-3) and briefings given here at Langley and at NASA Headquarters. The computer codes developed under this

contract were used extensively to guide the development of the LHS instrument.

SECTION 2 - OPTIMUM CHANNELS FOR SENSING STRATOSPHERIC TRACE GASES FROM SPACE

The intermediate frequency (IF) channels chosen for the LHS instrument were initially selected in a qualitative sense to minimize the errors in the retrieved concentrations of O_3 caused by random instrument noise. The original selection took into consideration the nature of molecular absorption in the atmosphere and the noise characteristics of the LHS. At high tangent altitudes narrow IF channels are needed to maximize the signal differential relative to a channel covering the wings of an absorption line. At lower tangent altitudes the line center may become completely opaque and thus useless in the retrieval. The retrieval than switches to a channel farther from line center that is not totally absorbed. The rolloff of the photodetector increases the noise present in a channel of fixed bandwidth as the channel moves away from line center. To counteract the signal degradation the channel bandwidth can be increased to offset the effects of the detector rolloff. Since the IF channels were chosen in a qualitative way based on an intuitive understanding of the instrument there is no guarantee that they are the optimum channels to use in the onion-peel retrieval process. The following section will discuss the studies performed to determine the optimum channels for O_3, $C\ell O$, HNO_3 and H_2O_2.

The retrieval process requires data from two IF channels at each tangent altitude. These two channels may be located

anywhere within the passband of the photomixer and may have any bandwidth. Bandwidth (BW) is defined as the width of the upper or lower sideband and the location of the channel is determined by the position of the sideband center relative to the local oscillator. IF frequency. A figure of merit (FOM) is defined from equation A-4 as

$$FOM = \frac{\varepsilon}{\ln(TR(H_t))} \alpha \begin{matrix} \text{Tangent Height Concentration} \\ \text{Relative Error} \end{matrix} \qquad (2\text{-}1)$$

where $TR(H_t)$ is defined by equation A-3. To calculate the FOM one first selects the bandwidths and locations of the two IF channels, calculates the channel averaged transmittance (to get $TR(H_t)$) and then calculates ε from the signal to noise ratios from the instrument model. Performing these calculations for a series of channel bandwidths and locations allows one to select an optimum pair of channels that minimizes the relative error in the retrieved concentration for each tangent altitude.

The calculational procedure was further simplified by fixing the location and bandwidth of one of the channels and varying the location and bandwidth of the other. To start, the location and bandwidth of the inner channel was set to 30 MHz and 40 MHz respectively. The location and bandwidth of the outer channel was varied from 150 to 900 MHz and 100 to 600 MHz respectively. For all four gases, the FOM was relatively insensitive to the combinations of IF channel location and bandwidth.

The location and bandwidth of the outer channel was than set to 800 MHz and 400 MHz respectively while the inner channel

parameters were varied. Because O_3 is a strong absorber (line center at 1129.4420 cm^{-1}) the FOM has a large variation over tangent altitude and channel parameters. Figs. 2-1 to 2-7 show the variation of FOM as a function of tangent height for a fixed bandwidth (BW, in MHz) while the channel location (DV, in MHz) is varied. Some general observations may be made. As the channel moves from the line center to the line wings the minimum in the FOM moves from high to low tangent altitudes. This is caused by the change in absorption line shape as a function of altitude. One can also see that as the bandwidth increases the FOM decreases. This is caused by the noise characteristics of the instrument, the larger the bandwidth the smaller the noise. From these figures one can construct a FOM response covering all tangent altitudes as shown in Fig. 2-8.

The channel bandwidths and locations obtained from this analysis are nearly identical to the set of five IF channels used to date. From Figs. 2-1 and 2-2 we can see that the smaller bandwidths give larger FOM's in the 50 to 60 km altitude region and would provide no advantage relative to the 40 MHz bandwidth selected. The dashed line in Fig. 2-8 shows a reasonable alternative to channels 1 and 2. While the FOM is decreased at 45 km it increases at 35 km and above 50 km. Given the constraint of not allowing the IF channels to overlap little improvement in the FOM can be achieved relative to the previously chosen IF filters. A second bank of IF filters would allow additional flexibility. Channels could be chosen in the second bank of filters to reduce the FOM at 45 and 35 km but from a

practical standpoint it is questionable whether the improvement in the retrieval would justify the additional expense and complexity. Atmospheric simulations and retrievals were carried out for ozone to validate these results. It was found in general that other channel combinations reduced the accuracy of the ozone retrievals.

The other gases; HNO_3, H_2O_2 and CℓO are weak absorbers and the interpretation of the FOM is much simpler. Figs. 2-9 to 2-11 give the tangent altitude variation of the FOM for HNO_3 (line center at 895.630 cm^{-1}). The FOM is a minimum at all altitudes when BW = 100 MHz. Figs. 2-12 to 2-14 give the tangent altitude variation of the FOM for H_2O_2 (line center at 1251.2602 cm^{-1}). The FOM is minimum and equal for BW = 20 MHz and 40 MHz above 35 km. From 12 to 30 km the FOM is equal for BW = 40 MHz and 100 MHz. Since channel overlap is not allowed the 40 MHz bandwidth would be the best choice. The situation for CℓO (line center at 856.499 cm^{-1}) is very similar as seen in Figs. 2-15 to 2-17. An inner channel with a bandwidth of 40 MHz would give the smallest FOM at the CℓO peak. Atmospheric simulations and retrievals were also carried out for these three gases. Combinations of channels other than the optimum pair were found to give poorer retrievals.

SECTION 3 - SPECTROSCOPIC DATA BASE

LHS is a high resolution instrument which measures the molecular absorption produced by a single line. To perform measurement feasibility studies or to reduce measurement data highly accurate line absorption parameters are required. Molecular line absorption can be accurately modeled when the line strength, Lorentz halfwidth, line position and lower state energy are known. The largest spectroscopic data base containing molecules of atmospheric interest is the AFGL line compilation. Over the course of this contract the accuracy of the data in this compilation has improved considerably and much new data has been added. Early LHS studies were based on the 1978 AFGL line compilation[4,5] augmented by line parameters for additional gases. Under this contract successive versions 1980[6], 1982[7,8] of the line compilation have been obtained and placed on the Langley computer system. The AFGL line compilation is split into two groups, a major gas and trace gas listing which are then merged into a single compilation for ease of use. The AFGL compilation is not the only source of line parameters. Many times other researchers have more accurate line parameters or line parameters not on the AFGL compilation. Programs were developed to strip old data (either positions, strengths or halfwidths) from the compilation and replace it with new data. For instance, a line compilation covering the microwave-millimeter region was obtained from a research group at JPL[9]. Overlapping data was removed from the main compilation and the microwave data was merged into the

main compilation. Data on HOCl was obtained from the National Bureau of Standards[10] and merged into the main compilation.

Spectral data on H_2O_2, $ClONO_2$ and N_2O_5 were purchased by the LHS project from the University of Denver. The data was taken with a .02 cm^{-1} and a .06 cm^{-1} resolution interferometer. Programs were developed under this contract to read the data tape, calculate the wave numbers corresponding to the amplitudes on the tape and plot the data versus wave number. $ClONO_2$ and N_2O_5 are both heavy molecules which tend to produce continuum type absorption. No distinct spectral features were found in either spectrum narrow enough to produce measurable differential absorption. Since neither one of these gases would be suitable for measurement by LHS no further analysis was carried out. H_2O_2 is however a much lighter molecule whose spectra exhibits spectral features produced by distinct absorption lines. Analysis was carried out to calculate the line positions and strengths of the H_2O_2 lines. To calculate the line position a parabola was fit to three data points at the minimum of the absorption line. The frequency where the parabola minimum occurs is calculated along with the amplitude at the minimum. A four point method, provided by the University of Denver, was also used because it has the capability to mark the shoulders of blended lines. Line strengths were determined by first calculating an integrated band strength and then apportioning the strength to individual lines based on the measured optical depth at line center. To determine the lower state energy would require a full quantum mechanical analysis which can not be done because of the

resolution of the data. Determination of the air broadened halfwidth is also not possible from the data on hand and in fact has not yet been measured. Figs. 3-1 to 3-3 show a small portion of the H_2O_2 spectrum. The measured spectrum and the calculated spectrum, based on the derived positions and strengths, are shown in the figure. The ability to reproduce the measured data is relatively good considering the level of analysis used here. The measured positions and strengths were combined with an assumed lower state energy of 200 cm^{-1} and an air broadened halfwidth of .1 cm^{-1}/atm to produce a data set suitable for simulating an LHS instrument signal. Additional laboratory measurements on H_2O_2 carried out with a tunable diode laser provided enough information to perform a full quantum mechanical analysis[11]. This improved H_2O_2 data set has been included in the current AFGL trace gas compilation.

The optimum spectral data set for the reduction of measurement data or the performance of measurement feasibility studies currently consists of the 1983 AFGL major gas and trace gas line compilations[7,8] augmented by some additional information for O_3 and CℓO in the 8 to 12 micron region. The CℓO line positions have been measured to five significant digits by Maki et al.[12]. Small spectral regions of the O_3 spectrum have been measured intensively by Hoell et al.[13] giving improved values for line positions, strengths and air broadened halfwidths. The CℓO and O_3 data have been placed on the Langley computer system for use in the LHS simulation programs as part of this contract.

SECTION 4 - THE EFFECT OF DIURNAL VARIATIONS ON THE RETRIEVED CONCENTRATIONS OF NO, NO_2 AND ClO FROM A SHUTTLE AND BALLOON BORNE MEASUREMENT PLATFORM

Work completed under this contract has resulted in a conference paper presented at the 1980 Quadrennial International Ozone Symposium[1]. The primary purpose of this work was to determine the feasibility of using a photochemical model to generate a set of diurnal correction curves. The present discussion extends the analysis for a space borne platform to a stratospheric balloon with a float altitude of 35 km and is an extension of work carried out in references 14 and 21.

In an occultation experiment such as LHS, one would ideally like to calculate the concentration at the tangent height. The ability to do this will be effected by concentration errors introduced at previous tangent heights and resolution errors caused by using discrete tangent heights in the retrieval algorithms. These types of errors produce a non-random bias error in the retrieved concentrations for a retrieval based on a noiseless instrument signal. Concentration errors caused by diurnal variations also produce constant bias errors and may be distinguished from errors due to other causes by comparing retrieved concentrations with and without the diurnal variations present. The logical vertical concentration profile to assume for the calculation of the synthetic transmittances when diurnal variations are absent is the 90° diurnal profile where the concentrations at other zenith angles are set equal to the 90°

value for a particular altitude. The overall calculation procedure is outlined in Table 1.

The retrieved concentrations for NO, NO_2 and CℓO from a measurement platform located in space are shown in Figs. 4-1 to 4-3 while Figs. 4-4 to 4-6 show the retrieved concentrations from a balloon platform at a float altitude of 35 km. Each figure contains six plots. The plot marked ρ_n in each figure is the vertical concentration profile when diurnal variations are absent. The curves marked ρ_n retrieved show how well the retrieval algorithm can infer the ρ_n profile.

The slight difference between ρ_n and ρ_n retrieved for the shuttle geometry in these figures can be attributed to resolution errors and to the use of slightly incorrect previously inferred concentration above a particular tangent height. The difference between ρ_n and ρ_n retrieved for the balloon geometry is much larger and can be attributed to using an average mixing ratio to model the optical mass above the balloon. The curves marked "uncorrected" indicate the size of the errors when no corrections are made in the retrieved algorithm for the diurnal variations. Large diurnal variations may occur in regions where the concentration is low and have little effect on the retrieved tangent height concentration. To more accurately quantify this, a mean factor for a tangent path, $\bar{R}$, may be defined as the ratio of the actual column density along the absorption path to the column density that would be present, assuming spherical symmetry, when using the distribution at 90^{o}. As expected from the calculated $\bar{R}$ of Fig. 6 in reference 11, which shows $\bar{R} < 1$ for

this case, the retrieved concentration is considerably smaller at lower tangent altitudes than the 90^{o} profile. The sharp drop off shown here occurs for several reasons. Notice that at the top of the atmosphere, where $\bar{R} \approx 1$, the correct tangent height concentration is calculated. At lower tangent altitudes however, $\bar{R} < 1$, and use of the previously calculated concentration will produce an optical depth larger than that which originally existed when the synthetic radiances were calculated. The retrieval algorithm attempts to counter this effect by decreasing the concentration being calculated at the current tangent height. At some point, however, the tangent height concentration will fail to counteract this effect with realistic positive concentrations and the retrieval algorithm will attempt to use negative concentrations, effectively defining a lower limit of useful information. The location of the lower limit is determined by the size of the optical depth error caused by the diurnal variation and the optical depth of the tangent height shell. When the optical depth error exceeds the optical depth of the tangent height shell the calculated concentration will be less than zero. Species whose concentration decreases with altitude will reach a lower useful limit at a higher altitude than those whose concentration increases. Although the LHS retrieval algorithm is based on differential absorption by ratioing the signal channel to the reference channel, the algorithm effectively becomes a direct absorption experiment because the outermost channel remains unattenuated for the trace species shown here. If this were not true the above argument

concerning the cause of the rapid dropoff of the retrieved concentration would have to be extended to include the effects of the concentration variation as a function of zenith angle. For the opposite case where $\bar{R} > 1$ at lower tangent altitudes, the retrieved concentration will be overestimated because the calculated optical depth will be smaller than the original optical depth. The overestimation does not produce as dramatic a change in the retrieval results as does the underestimation.

Curves marked "corrected" illustrate the resulting retrieval when the diurnal variations are known precisely and diurnal corrections can be made exactly in the retrieval algorithm. For the shuttle geometry there is little difference between "ρ_n retrieved" and the "corrected" results. Significant differences can be seen between these two cases for the balloon geometry. This is caused by the fact that the optical mass is proportioned differently above and below the balloon depending on whether the ρ_n distribution or the full diurnal distribution is used. Also shown in these figures are curves marked E^+ and E^-. These indicate the expected range of uncertainty in the retrieved concentration caused by uncertainties in the diurnal correction factors. The uncertainties in the diurnal correction factors used here are based on photochemical model calculations which are fully described in Reference 1. The error envelope produced by the uncertainties in the diurnal correction factors show that photochemical model predictions of the diurnal correction factors can improve retrieval results for measurements from both a shuttle and balloon platform. Measurements from a balloon

platform suffer from an additional error source, the assumption of a constant mixing ratio above the balloon. This retrieval error varies as a function of the solar zenith angle used to infer the average mixing ratio and in some cases the resulting error can be greater than that due to uncertainties in the diurnal correction factors.

TABLE 1

CALCULATION PROCEDURE FOR EACH TARGET GAS

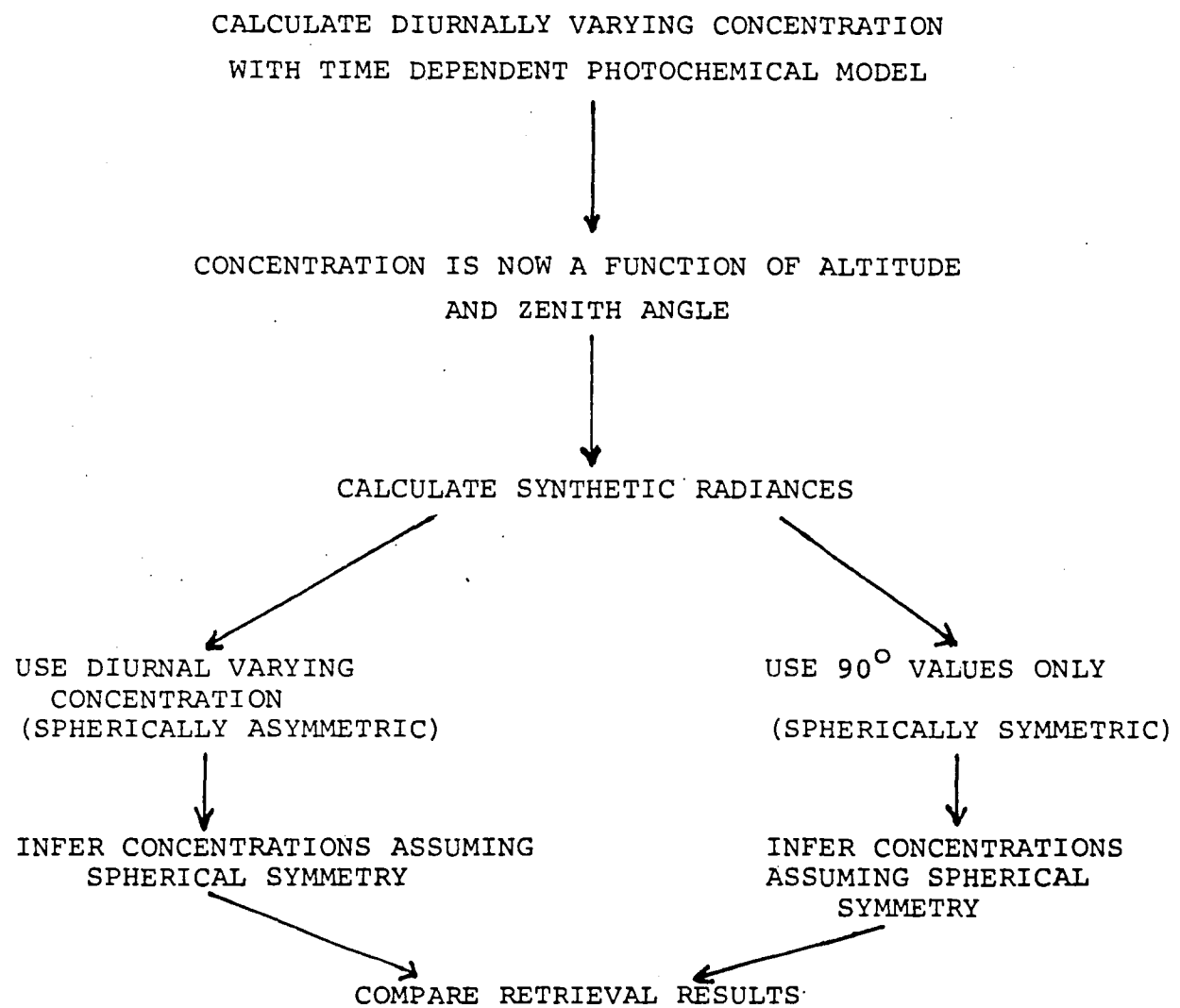

SECTION 5 - LHS INSTRUMENT CONTROL SOFTWARE

Considerable software development was carried out for all levels of the LHS instrument in both Fortran and assembly code. The overall design philosophy for the LHS instrument is described in reference 2. The majority of this work was concerned with development at the subsystem level.

Master control of the instrument resides with the channel control unit which consists of a Texas Instrument TMS-990 16 bit microprocessor. An RS-232C serial link was chosen for the communication link between the channel control unit and slave subsystems. The slave subsystems consist of a standard 8 bit interface bus and an 8085 microprocessor. Under this contract master/slave protocol was developed and operational software for the microprocessor based subsystems was developed in assembler code for the output control unit, current and temperature control unit, receiver data acquisition unit, motor control unit, manual motor control unit, channel control unit and the engineering data acquisition subsystem. Test procedures were developed and carried out for each subsystem in the laboratory setting and also in the flight configuration. Documentation of the slave subsystems includes user's guides, detailed programming guides and configuration charts. These have been delivered to the LHS project. Procedures used to generate code in the EPROM's placed in the subsystems were also documented. A boot loader for the TI-990 was developed in assembly code to provide stand alone capability for the flight channel control units.

SECTION 6 - LHS SOFTWARE DEVELOPMENT

Figure 6-1 is a flow chart of some of the data analysis software developed under this contract to analyze the instrument data. Instrument data is written on 1600 BPI magnetic tape in two's complement hexadecimal. Recorded data is grouped into 8 records, corresponding to the origin of the data. Each record contains an internal identifier since there is no guaranteed order in which they will appear on tape. The 8 records consist of the heterodyne record, wavelength identification record, heterodyne and wavelength ID records cross-strapped from the other channel control unit, an instantaneous data record, an engineering data record, description record and a pointer tracker record which will rarely be seen. The heterodyne and wavelength identification records may be blocked into groups of eight to conserve magnetic tape and also to prevent buffer overflows in the output control unit.

Data analysis begins with program LTCOPY. NOS system software is used to convert the 8 bit characters to compatible 6 bit CDC characters while copying the data to disk. Program JCRAK performs all of the record decoding. The records are buffered in, identified, unblocked if necessary, hexadecimal numbers are converted to decimal, the two's complement conversion is performed and the decoded records are written to an output file. Each record is checked for proper length, illegal characters, out of place separators or missing record delimiters. Each record is processed sequentially and this order

is maintained in the output file. JPAS2 reads through this file searching for commands from the TI software programs. This print out gives the time history of the data on the tape and allows the user to identify different groups of data. This program also checks the error flags in each record and prints out each occurrence. If the data was cross strapped from the other channel control unit there will be no TI-990 commands in the file. Program JSWEEP allows the user to search the data file looking for certain characters; for example, a time difference between adjacent records greater than 2 seconds could mark the ending and starting times for two consecutive line extraction scans. At this point the user may plot up to seven of the variables contained in the data records as a function of time with program JQPOT. This gives the user a quick look at the data and identifies any major problems with the data. If the user requested more than 1 sample/frequency point in any of the scan modes program JCOND must be run to calculate an average value for each variable at that frequency point. Scans of the same spectral region can be coadded with program JCOAD. The output data is no longer sequentially stored. Program JCPOT plots the original scan and the coadded scans to that point. Program REDO takes the coadded spectra and reformats the data into a form compatible with a spectral data base developed for the analysis of interferometer spectra. Once the data is in this format many other programs, such as those that mark line positions, calculate equivalent widths and specialized plotting programs can be used to analyze the data. Some additional programs (Fig. 6-2) have

been developed to analyze and validate the data that are not part of the standard data reduction process. Program JSTAB calculates running means and standard deviations to check the instrument stability. It can also be used to calculate signal to noise ratios, zero levels and black body calibration levels. Program LHSRET retrieves concentration profiles from data taken in either the locked or scan modes using the weighting function retrieval algorithm in reference 16. Program LHSFIT performs a non-linear least squares fit to laboratory data. The user may fit the spectrum background, line positions, strengths and halfwidths for several lines. It is based on a program developed by C. P. Rinsland to analyze interferometer data. The program was modified to handle non-uniform point spacing, the LHS IF filters and generalized to handle the twenty eight gases contained on the AFGL line compilation. Program TDLCHAR plots the data taken by the TI-990 CL2 program. It shows the TDL lasing mode locations as a function of wavelength for different temperature and current settings. Program JBIG normalizes the background amplitudes to 1 and expands the vertical plotting scale in order to identify weak absorption features.

The remainder of the software developed under this contract is listed in Figure 6-3. All of the computer codes are residing on the NASA/LaRC computer system. Complete listings of the codes have been provided to the government as part of this contract.

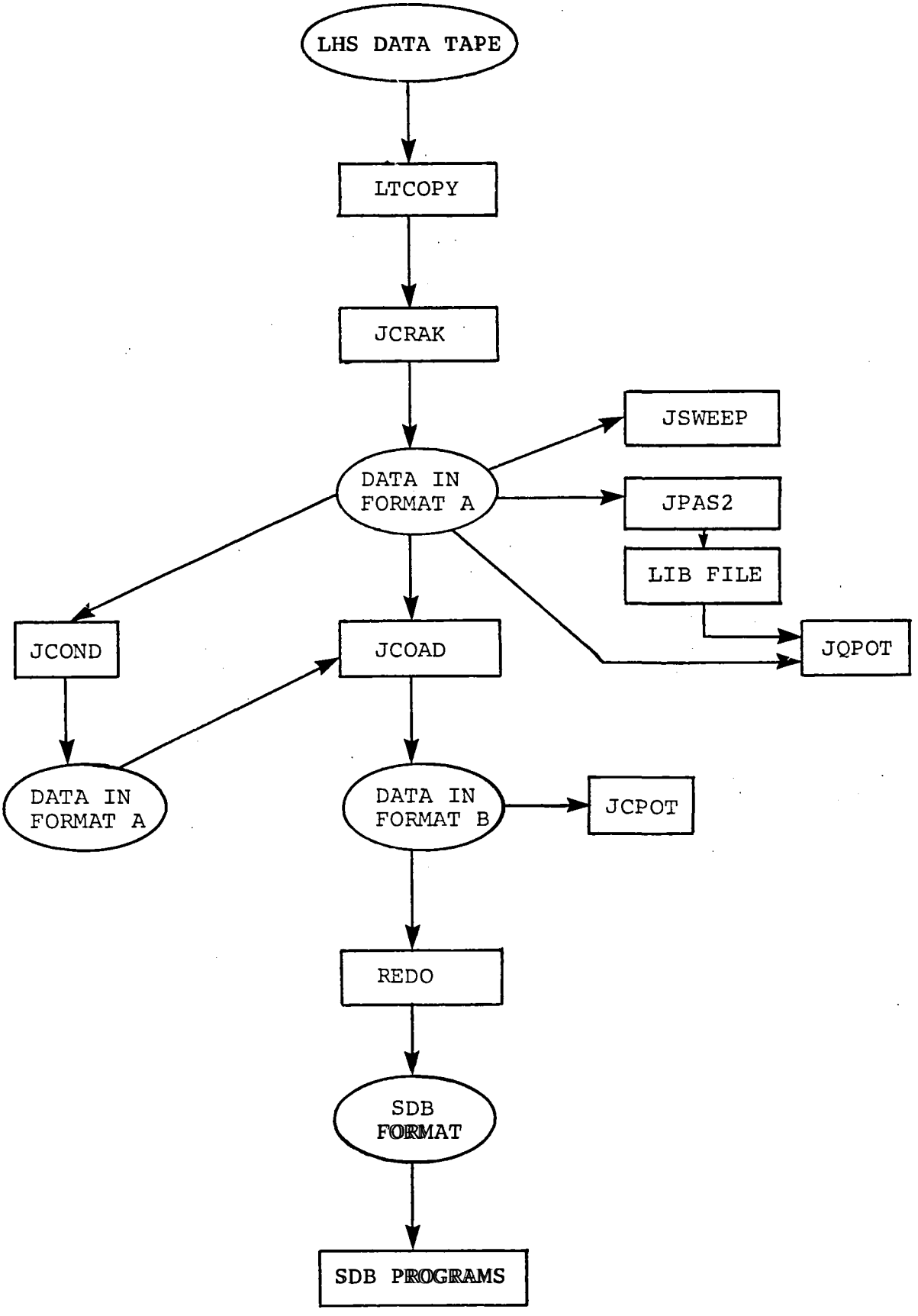
LHS DATA TAPE
LTCOPY
JCRAK
JSWEEP
DATA IN FORMAT A
JPAS2
LIB FILE
JQPOT
JCOND
JCOAD
DATA IN FORMAT A
DATA IN FORMAT B
JCPOT
REDO
SDB FORMAT
SDB PROGRAMS

Figure 6-1

DATA FORMAT	PROGRAM
B	JSTAB
A, B	LHSRET
A, B	LHSFIT
A	TDLCHAR
B	JBIG

Figure 6-2

NAME	FUNCTION
BFRACT	Calculate atmospheric refraction.
BOB	Inverts diurnal distribution so zenith angle increases with array location.
BPLOT	Plots diurnal variation of gas concentration vs. time for any gas.
CELPLOT	Calculates and plots cell monochromatic transmittances.
DRET	LHS onion peel retrieval for diurnally varying gas.
DRETN	LHS onion peel retrieval for diurnally varying gas with upper altitude correction.
DURNC	Remote selected diurnally varying gas from data base.
DURNPR	Print out diurnal variation of specified gas.
FASATR	FASCOD1B atmospheric model modified to calculate mass paths of a diurnally varying gas.
INST	LHS instrument model.
INSTSIM	LHS instrument model with grating losses, excess noise and detector rolloff.
JPLREAD	Read JPL SUBMM tape.
LHSRET	LHS weighting function retrieval program.
LIMPOTF	Calculate atmospheric transmittances.
LIMPOTP	Calculate atmospheric transmittances and plot normalized transmittances.
LIMSMO	Calculate atmospheric transmittances with LHS instrument model.
M1982	Merges major and trace AFGL line compilations.

Figure 6-3

NAME	FUNCTION
NDIURN	Perform simulation and retrieval for a diurnally varying gas with LHS instrument model.
PRET	Performs onion peel retrieval of diurnally varying gas including diurnal correction factor.
RET	LHS onion peel retrieval.
SANDM	Sorts and merges two line files.

Figure 6-3

SECTION 7 - REFERENCES

1. Larsen, J. C. and R. E. Boughner, The Feasibility of Using Time-Dependent Photochemical Calculations to Infer Radical Species Concentrations From Solar Occultation Absorption Measurements. Proc. Quadrennial Int. Ozone Symp., Vol. II, edited by J. London, pp. 948-955, IAMAP, Boulder, CO., 1980.

2. Shull, T. A., and P. L. Rinsland, Automated Control and Data Acquisition for a Tunable Diode Laser Heterodyne Spectrometer. Collection of Technical Papers of the AIAA Computers in Aerospace IV Conference, Hartford, CONN., 235, October, 1983.

3. Alvarez, J. M., J. C. Larsen, and W. P. Chu, The Upcoming Test Flight of a Laser Heterodyne Spectrometer, Topical Meeting in Optical Techniques for Remote Probing of the Atmosphere, Jan. 10-12, 1983, Incline Village, NEV.

4. Rothman, L. S. Update of the AGFL Atmospheric Absorption Line Parameter Compilation. Applied Optics, 17, 22, 3517-3518, 1978.

5. Rothman, L. S., S. A. Clough, R. A. McClatchey, L. G. Young, D. E. Snider, and A. Goldman. AFGL Trace Gas Compilation, Applied Optics, 17, 4, 507, 1978.

6. Rothman, L. S., AFGL Atmospheric Absorption Line Parameters Compilation: 1980 Version. Applied Optics, 20, 5, 791-795, 1981.

7. Rothman, L. S., R. R. Gamache, A. Barbe, A. Goldman, J. R. Gillis, L. R. Brown, R. A. Toth, J.-M. Flaud and C. Camy-Peyret. AFGL Atmospheric Absorption Line Parameters Compilation: 1982 Edition, Applied Optics, 22, 15, 2247-2256, 1983.

8. Rothman, L. S., A. Goldman, J. R. Gillis, R. R. Gamache, H. M. Pickett, R. L. Poynter, N. Husson and A. Chedin. AFGL trace gas compilation: 1982 Version. Applied Optics, 22, 11, 1616-1627, 1983.

9. Poynter, R. L. and H. M. Pickett, Submillimeter, and Microwave Spectral Line Catalogue. JPL Publication 80-23, 1980.

10. Sams, R. L. and W. B. Olson, Analysis of the High-Resolution Infrared Spectrum of the ν_2 Bending Mode of HOCℓ at 1238 cm^{-1}. J. Molecular Spectroscopy, 84, 113-123, 1980.

11. Hillman, J. J., D. E. Jennings, W. B. Olson and A. Goldman, A Combined FTS/TDL Study of H_2O_2 - the ν_6 Fundamental. High Resolution Infrared Applications and Developments, National Bureau of Standards, Gaithersburg, MD., June 23-25, 1980.

12. Maki, A. G., F. J. Lovas, and W. B. Olson, Infrared Frequency Measurements on the CℓO Fundamental Band. J. Mol. Spec., 92, 410, 1982.

13. Hoell, J. M., C. N. Harward, C. H. Bair, and B. S. Williams, Ozone Air Broadening Coefficients in the 9 μm Region. Optical Engineering, 1982.

14. R. E. Boughner, J. C. Larsen and M. Natarajan, The Influence of NO and CℓO Variations at Twilight on the Interpretation of Solar Occultation Measurements, Geophysical Research Letters, 7, 4, 231-234, 1980.

15. Hoell, J. M., J. S. Levine, T. R. Augustsson, and C. N. Harward, Atmospheric Ammonia: Measurements and Modeling, AIAA Journal, 20, 88, 1982.

16. Goldman, A. and R. S. Saunders, Analysis of Atmospheric Infrared Spectra for Altitude Distribution of Atmospheric Trace Constituents-I. Method of Analysis. J. Q. S. R. T., V21, 155-161, 1979.

17. Russell, J. M. and S. R. Drayson, The Inference of Atmospheric Ozone Using Satellite Horizon Measurements in the 1042 cm^{-1} Band. J. Atmos. Sci., 29, 376-390, 1972.

18. McKee, T. B., R. I. Whitman, and J. J. Lambiotte, Jr., A Technique to Infer Atmospheric Water-Vapor Mixing Ratio from Measured Horizon Radiance Profiles. NASA TN D-5252, 1969.

19. Tallamaraju, R. K., Inference of Stratospheric Minor Constituents from Satellite Limb Radiant Intensity Measurements, ORA Project 011023 College of Engineering, Univ. of Michigan, 1975.

20. Siegman, A. E., The Antenna Properties of Optical Heterodyne Receivers, Proc. of the IEEE, 54, 1350-1356, 1966.

21. Larsen, J. C., Analysis of a Laser Heterodyne Spectrometer, Sept. 1980, NASA CR-159319.

SECTION 8 - FIGURES

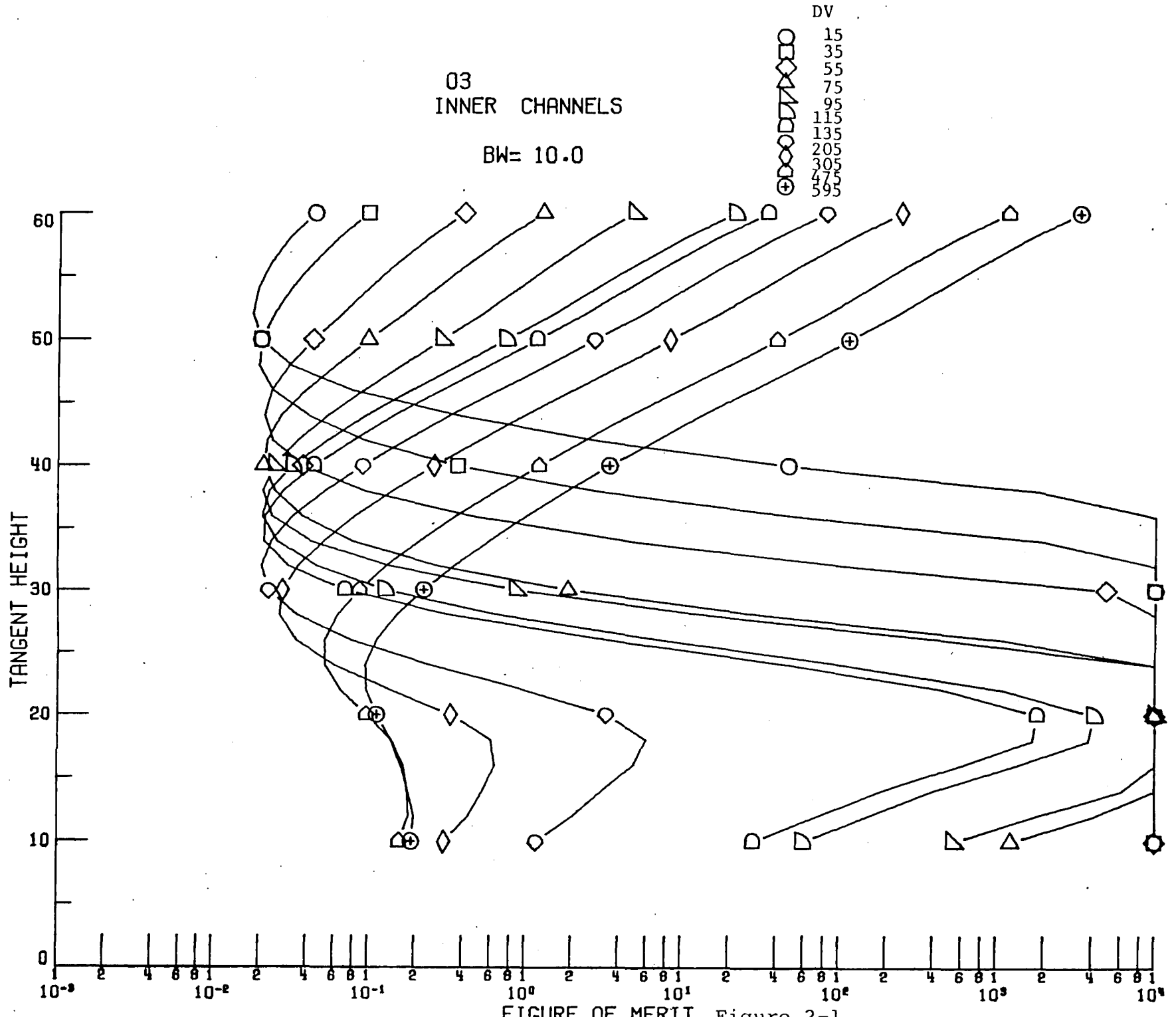
03
INNER CHANNELS
BW= 10.0
DV
15
35
55
75
95
115
135
205
305
475
595
TANGENT HEIGHT
60
50
40
30
20
10
0
FIGURE OF MERIT

Figure 2-1

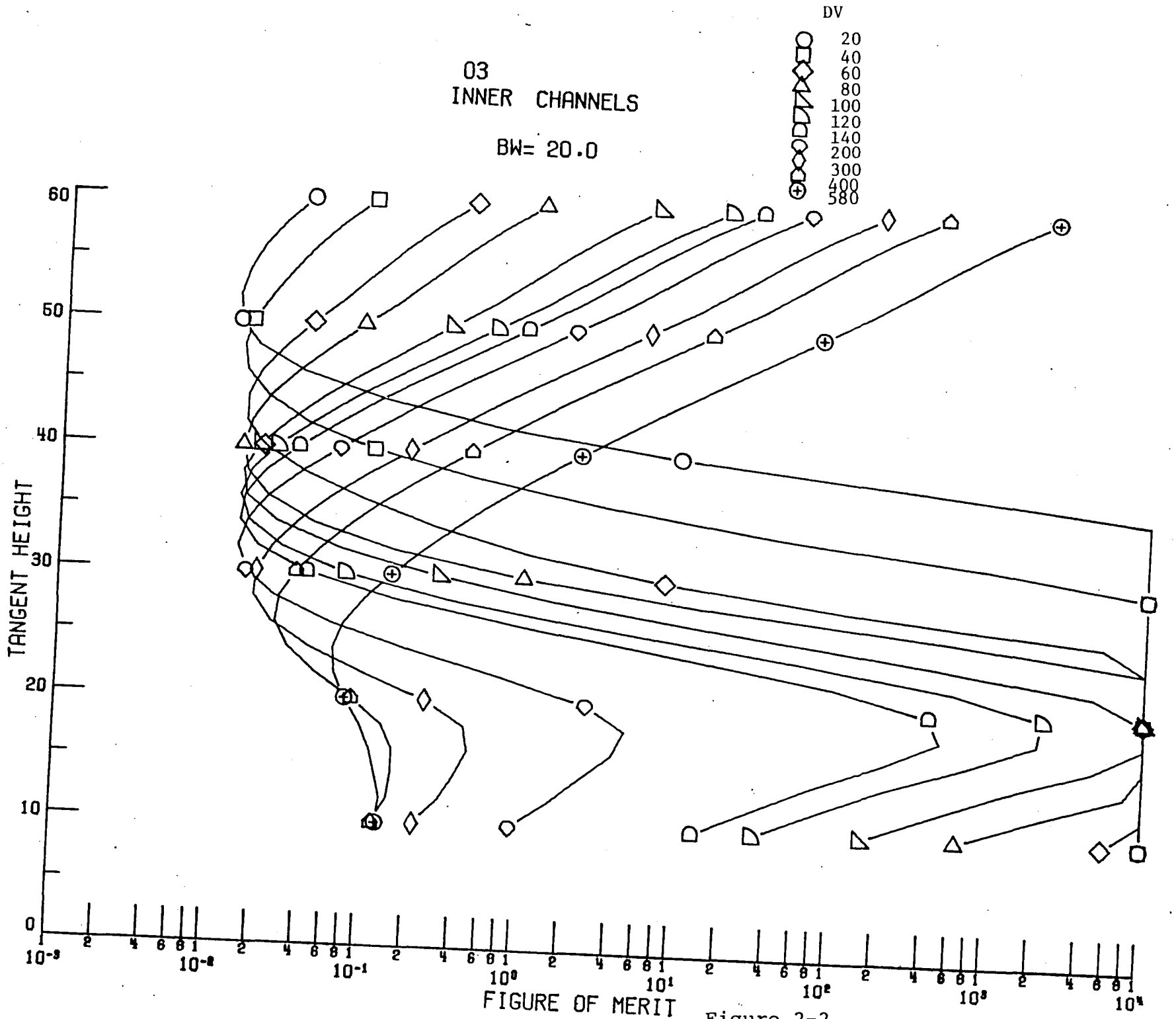
03
INNER CHANNELS
BW= 20.0
DV
20
40
60
80
100
120
140
200
300
400
580
TANGENT HEIGHT
60
50
40
30
20
10
0
10⁻³
10⁻²
10⁻¹
10⁰
10¹
10²
10³
10⁴
FIGURE OF MERIT

Figure 2-2

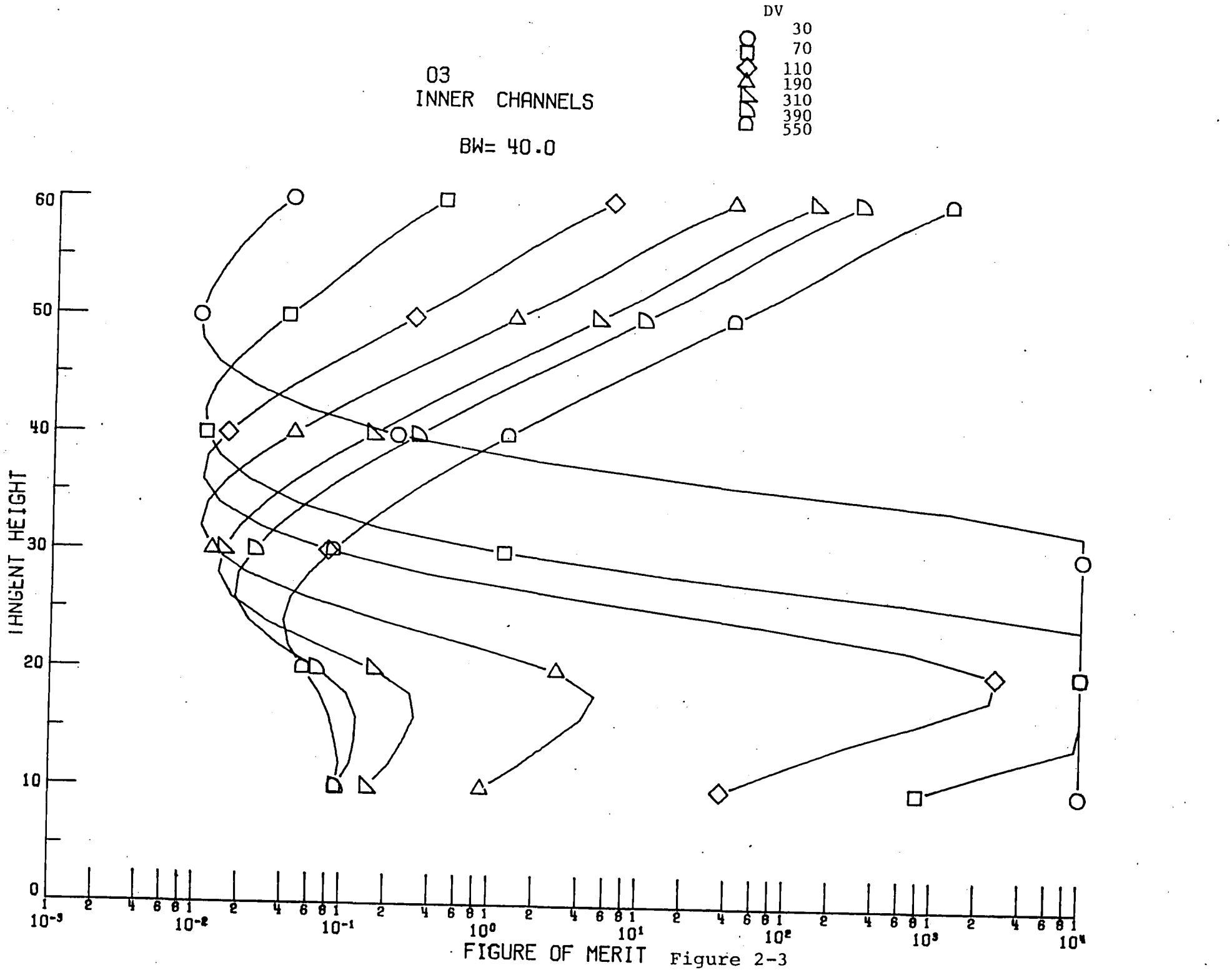
DV
30
70
110
190
310
390
550
03
INNER CHANNELS
BW= 40.0
TANGENT HEIGHT
60
50
40
30
20
10
0
10^{-3}
10^{-2}
10^{-1}
10^{0}
10^{1}
10^{2}
10^{3}
10^{4}
FIGURE OF MERIT

Figure 2-3

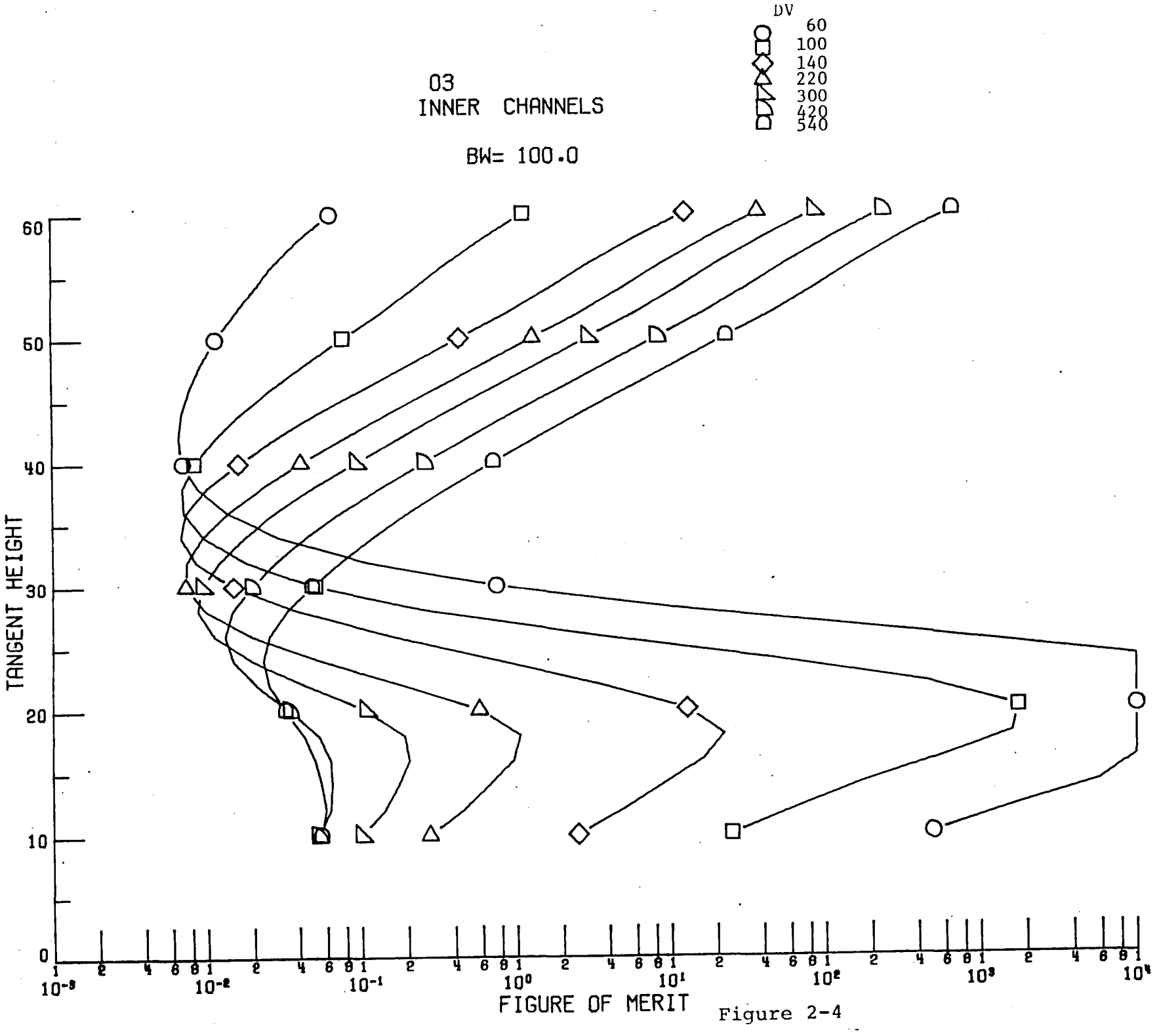
03
INNER CHANNELS
BW= 100.0
DV
60
100
140
220
300
420
540
TANGENT HEIGHT
60
50
40
30
20
10
0
FIGURE OF MERIT

Figure 2-4

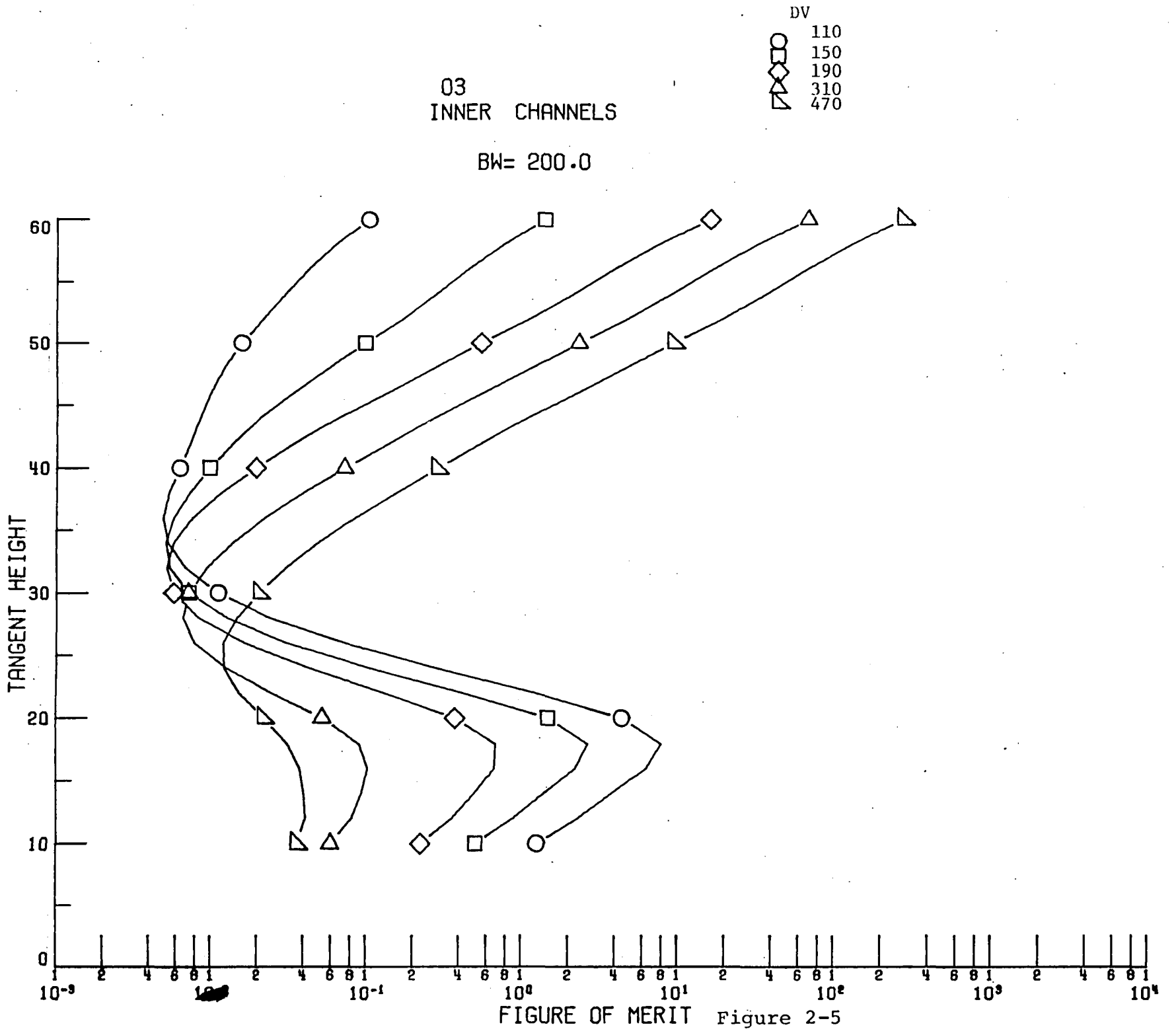
DV
110
150
190
310
470
03
INNER CHANNELS
BW= 200.0
TANGENT HEIGHT
60
50
40
30
20
10
0
10⁻¹
10⁰
10¹
10²
10³
10⁴
FIGURE OF MERIT

Figure 2-5

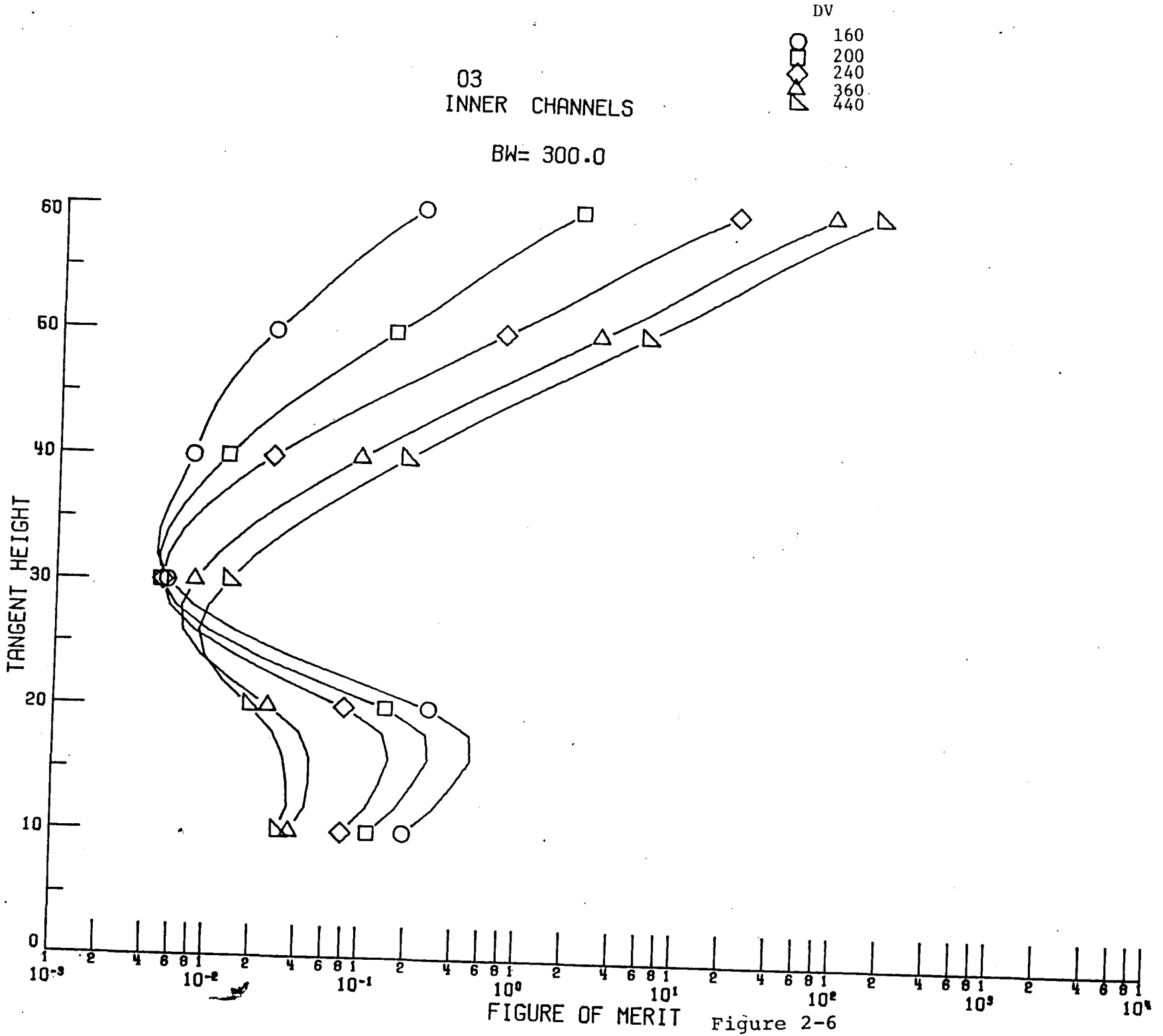
DV
160
200
240
360
440
03
INNER CHANNELS
BW= 300.0
TANGENT HEIGHT
60
50
40
30
20
10
0
FIGURE OF MERIT

Figure 2-6

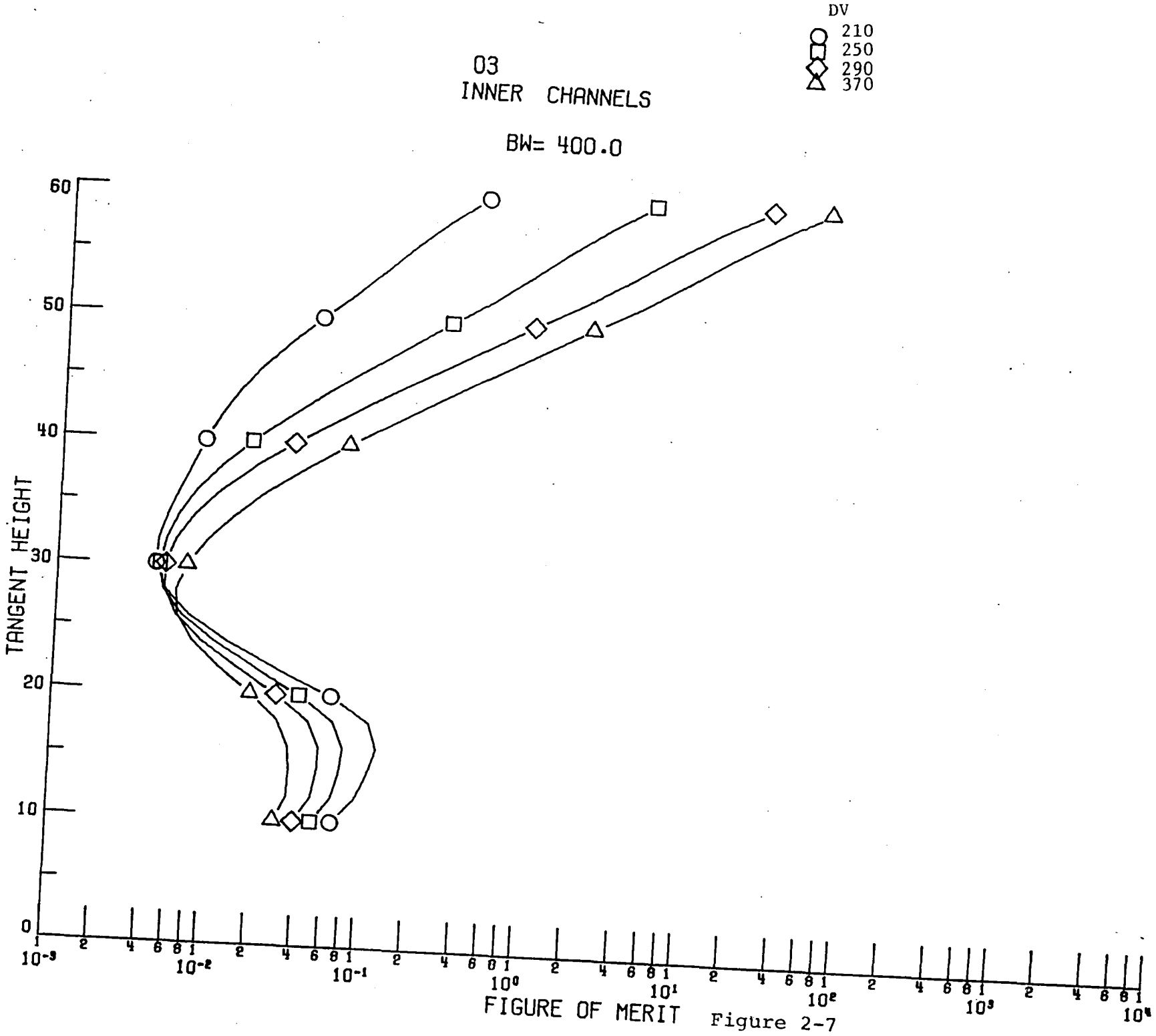
DV
210
250
290
370
03
INNER CHANNELS
BW= 400.0
TANGENT HEIGHT
60
50
40
30
20
10
0
FIGURE OF MERIT

Figure 2-7

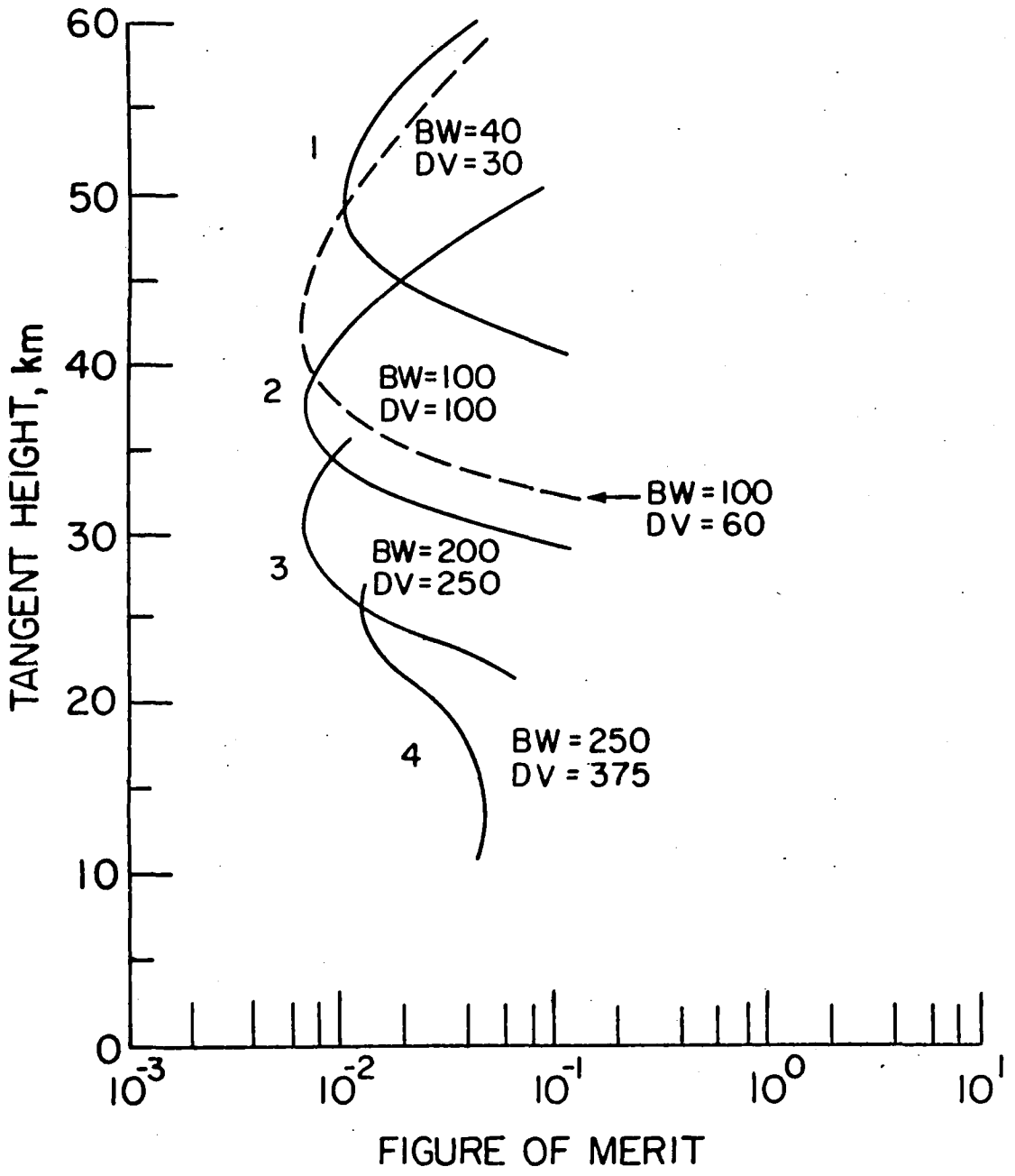
60
50
40
30
20
10
0
TANGENT HEIGHT, km
1
BW=40
DV=30
2
BW=100
DV=100
BW=100
DV=60
3
BW=200
DV=250
4
BW=250
DV=375
10^{-3}
10^{-2}
10^{-1}
10^{0}
10^{1}
FIGURE OF MERIT

Figure 2-8

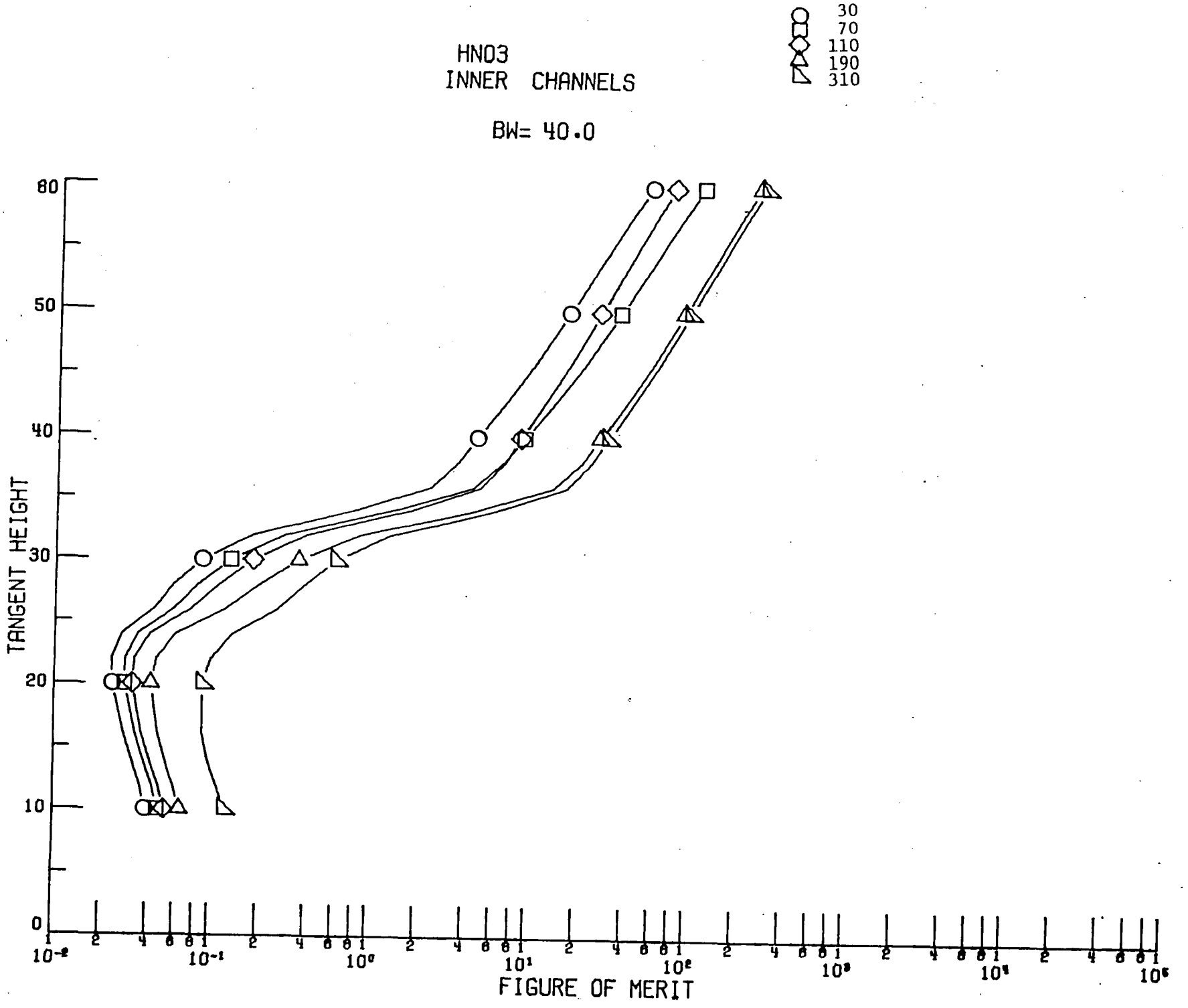
HNO3
INNER CHANNELS
BW= 40.0
30
70
110
190
310
TANGENT HEIGHT
FIGURE OF MERIT

Figure 2-9

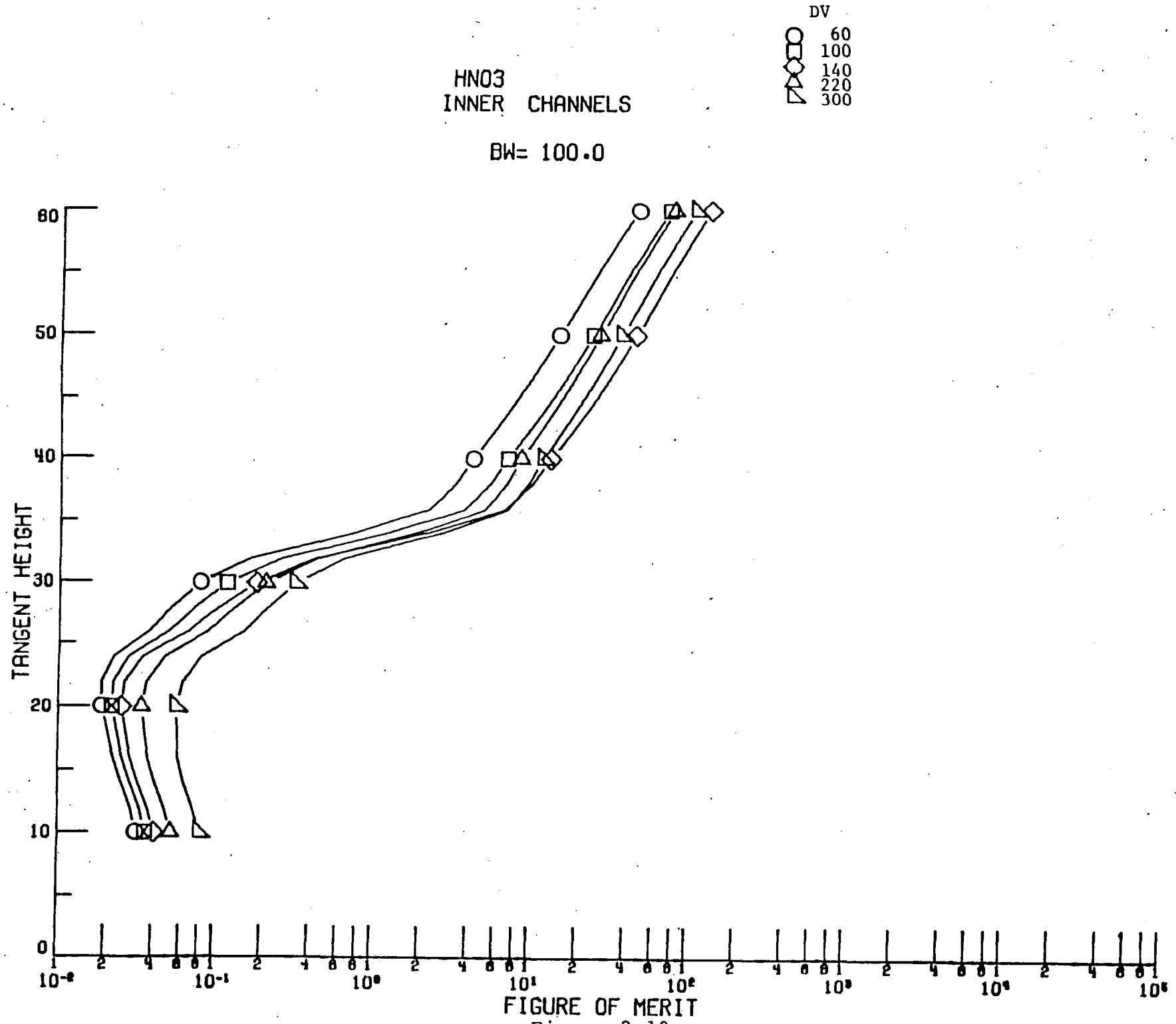
DV
60
100
140
220
300
HN03
INNER CHANNELS
BW= 100.0
TANGENT HEIGHT
0
10
20
30
40
50
60
FIGURE OF MERIT

Figure 2-10

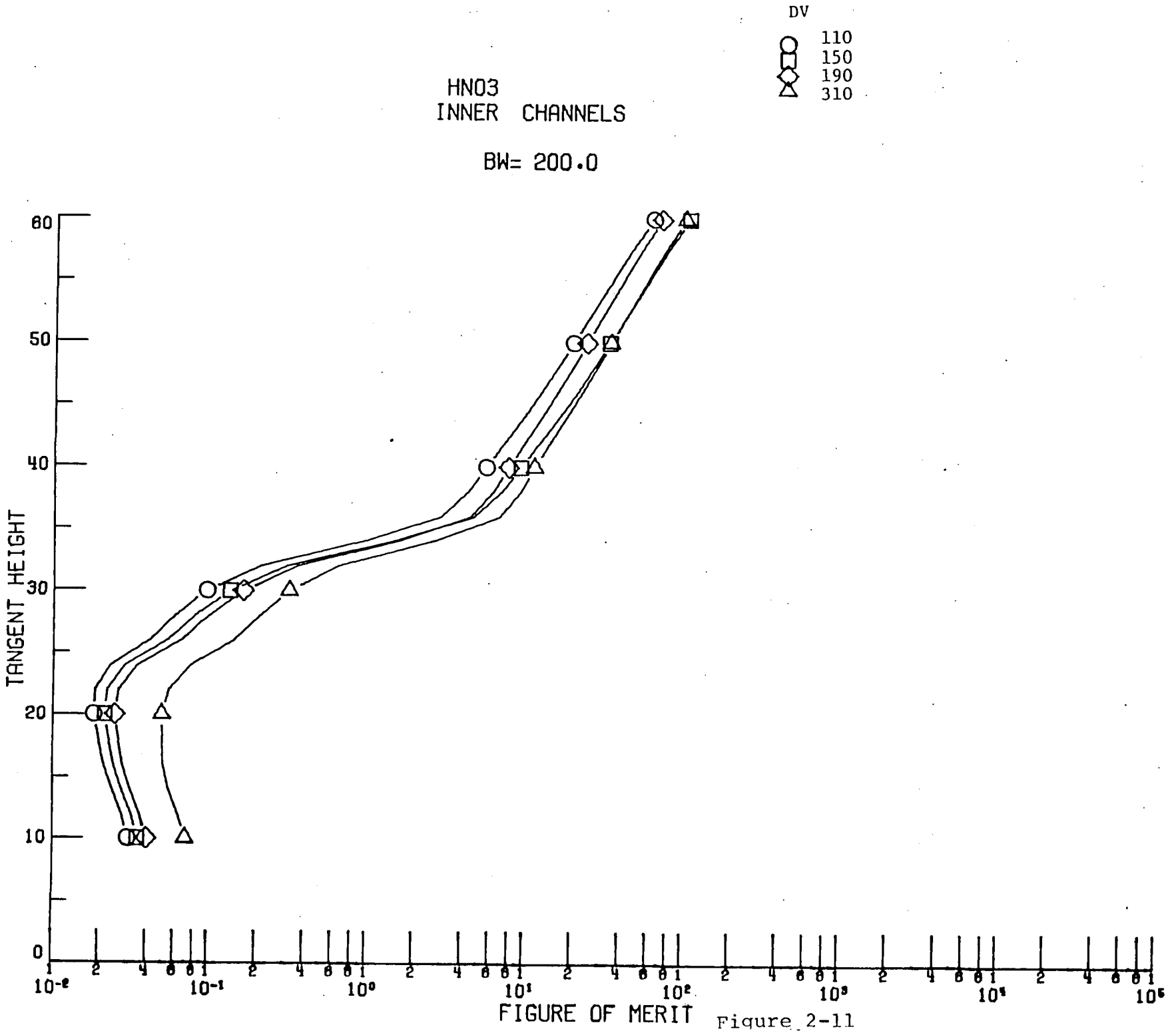
DV
110
150
190
310
HN03
INNER CHANNELS
BW= 200.0
TANGENT HEIGHT
60
50
40
30
20
10
0
10⁻²
10⁻¹
10⁰
10¹
10²
10³
10⁴
10⁵
FIGURE OF MERIT

Figure 2-11

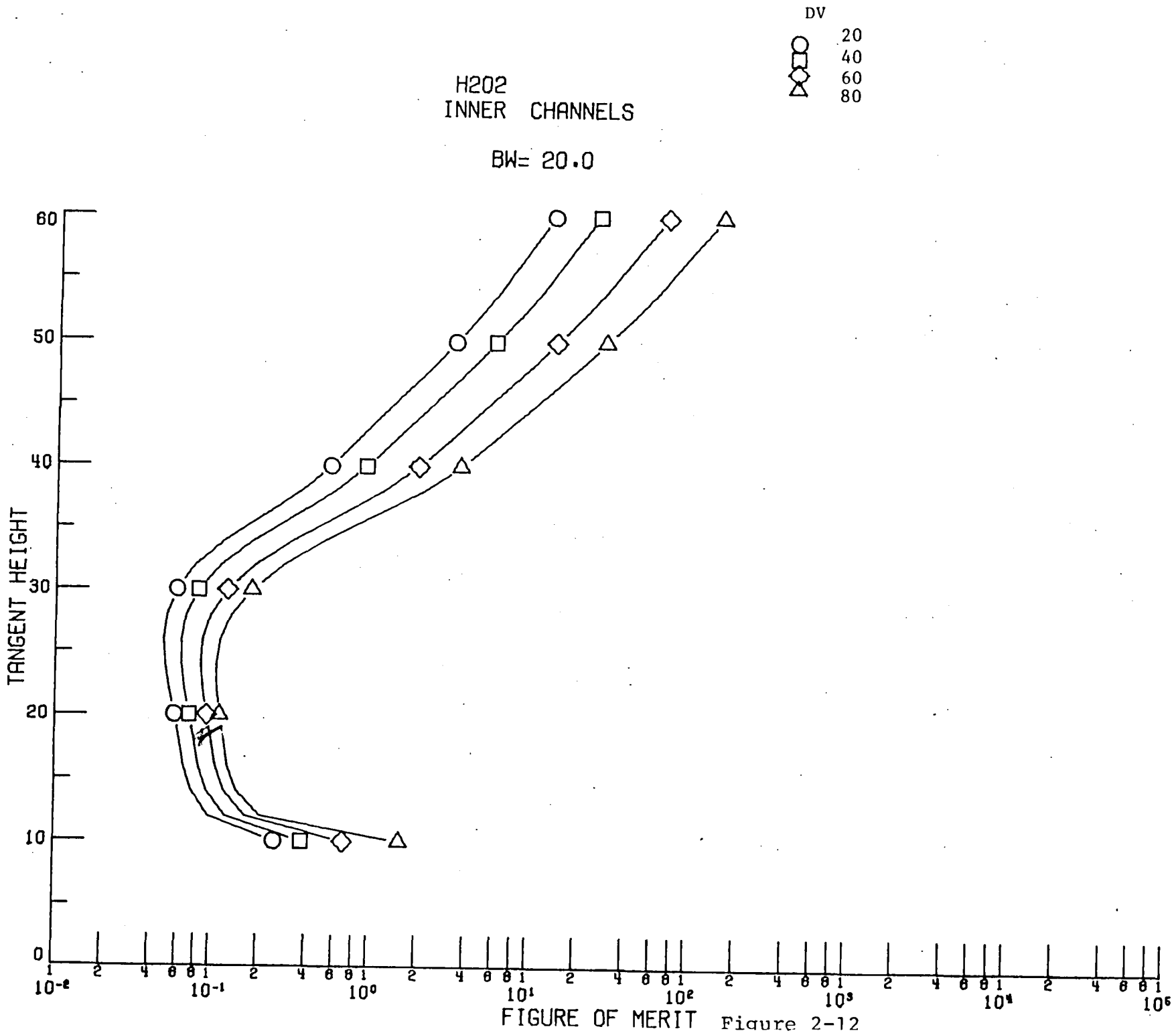
DV
20
40
60
80
H202
INNER CHANNELS
BW= 20.0
TANGENT HEIGHT
60
50
40
30
20
10
0
FIGURE OF MERIT

Figure 2-12

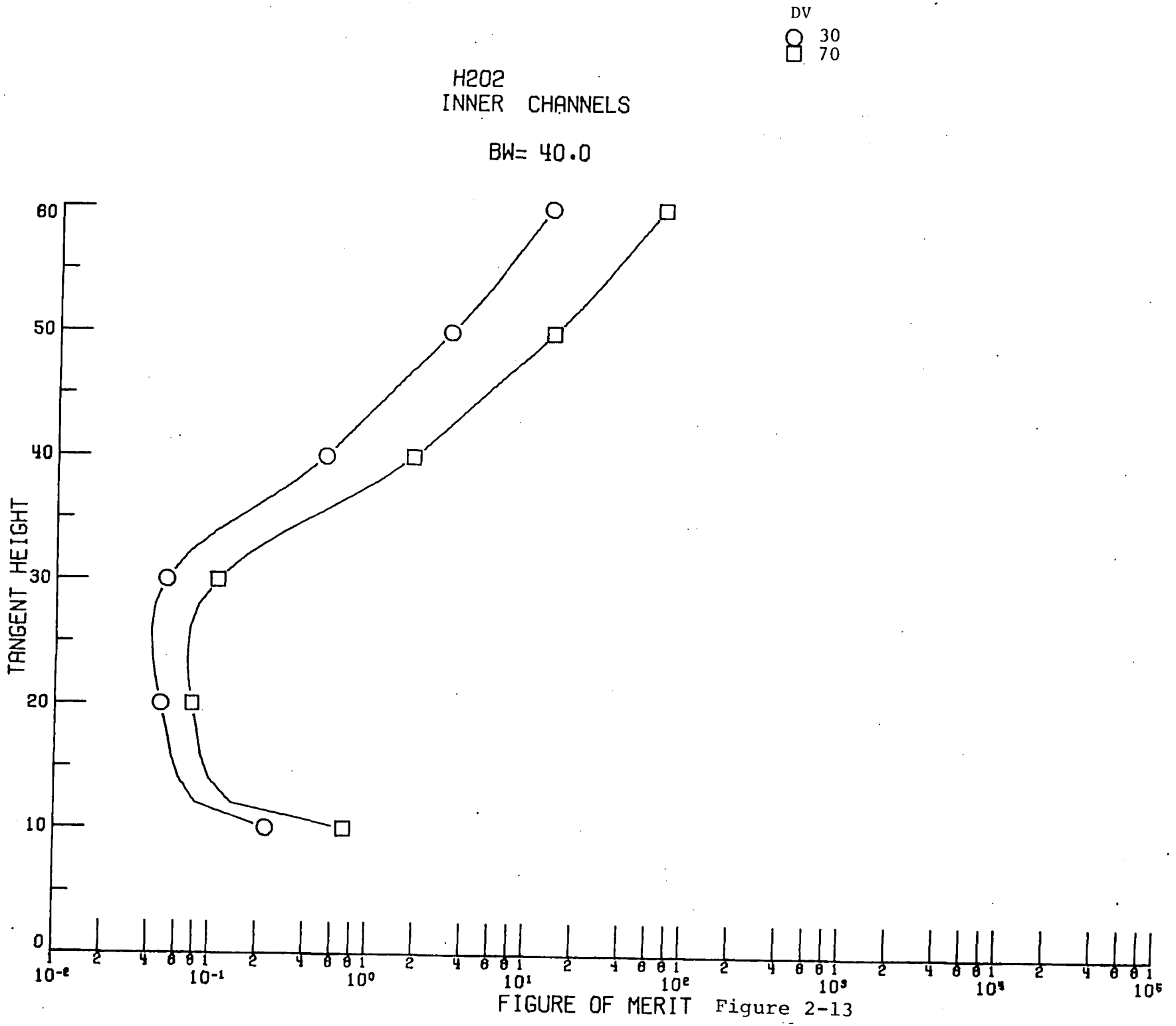
DV
30
70
H202
INNER CHANNELS
BW= 40.0
TANGENT HEIGHT
60
50
40
30
20
10
0
10⁻²
10⁻¹
10⁰
10¹
10²
10³
10⁴
10⁵
FIGURE OF MERIT

Figure 2-13

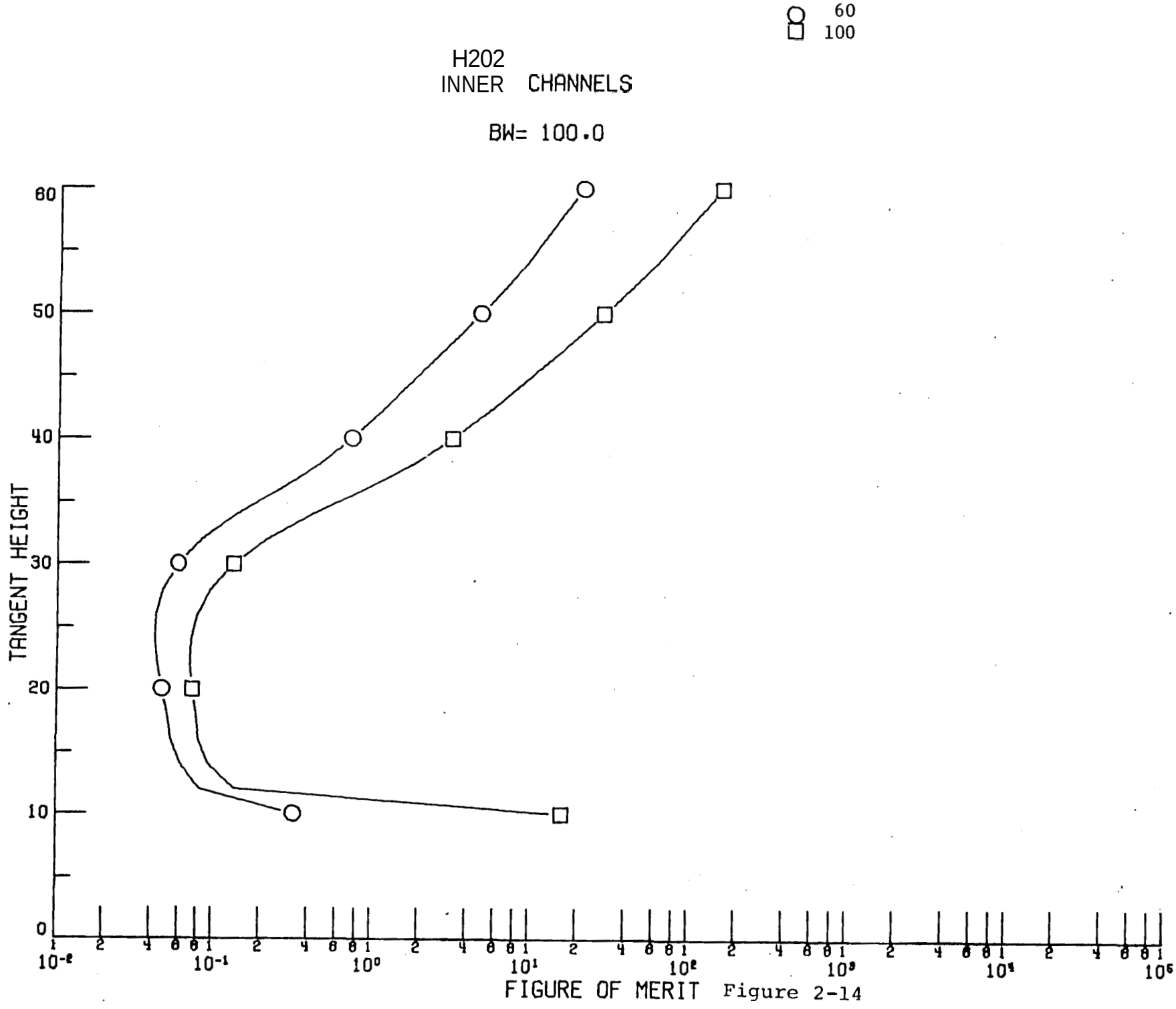
60
100
H202
INNER CHANNELS
BW= 100.0
TANGENT HEIGHT
60
50
40
30
20
10
0
10⁻²
10⁻¹
10⁰
10¹
10²
10³
10⁴
10⁵
FIGURE OF MERIT

Figure 2-14

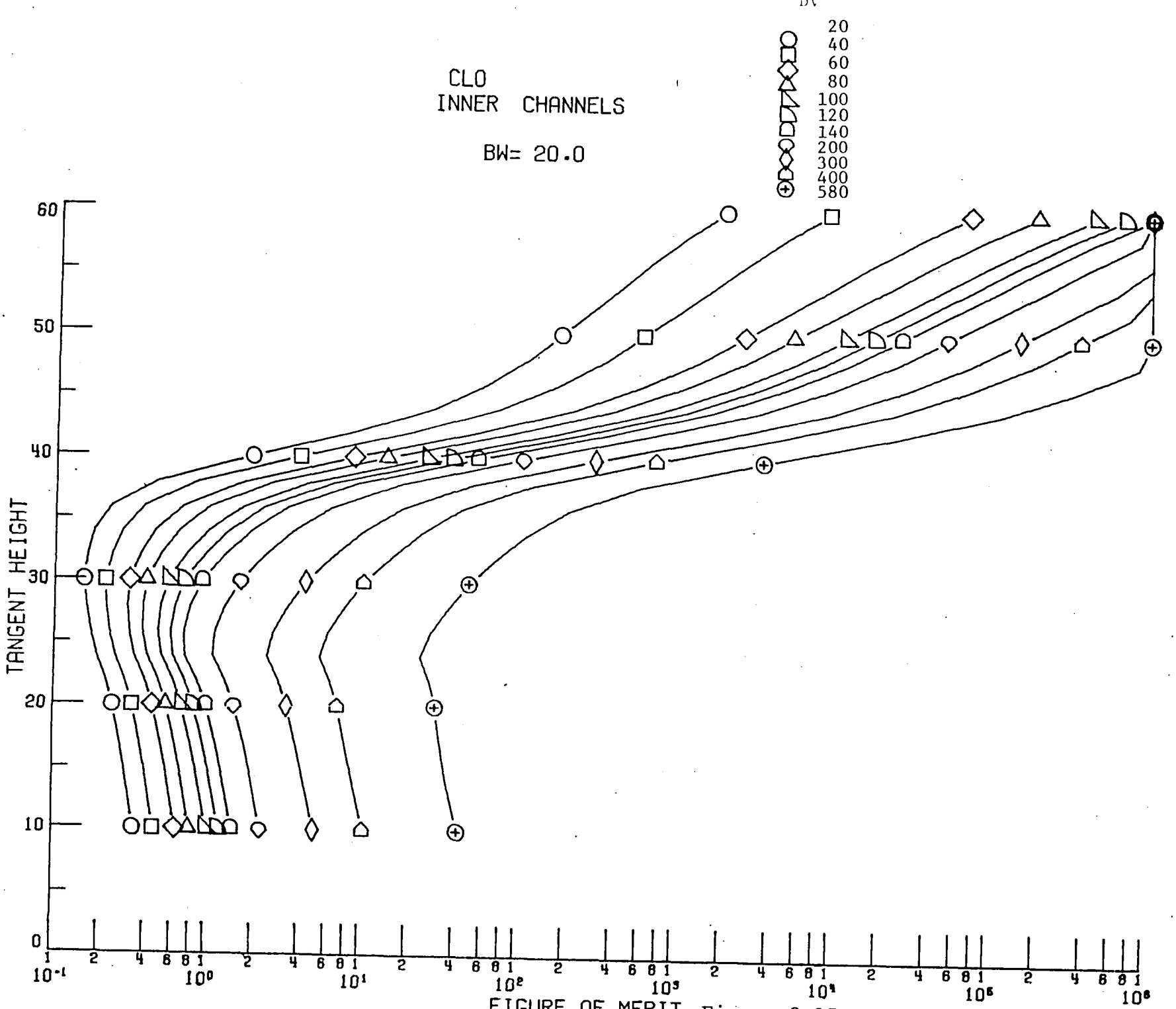
CLO
INNER CHANNELS
BW= 20.0
DV
20
40
60
80
100
120
140
200
300
400
580
TANGENT HEIGHT
60
50
40
30
20
10
0
10⁻¹
10⁰
10¹
10²
10³
10⁴
10⁵
10⁶
FIGURE OF MERIT

Figure 2-15

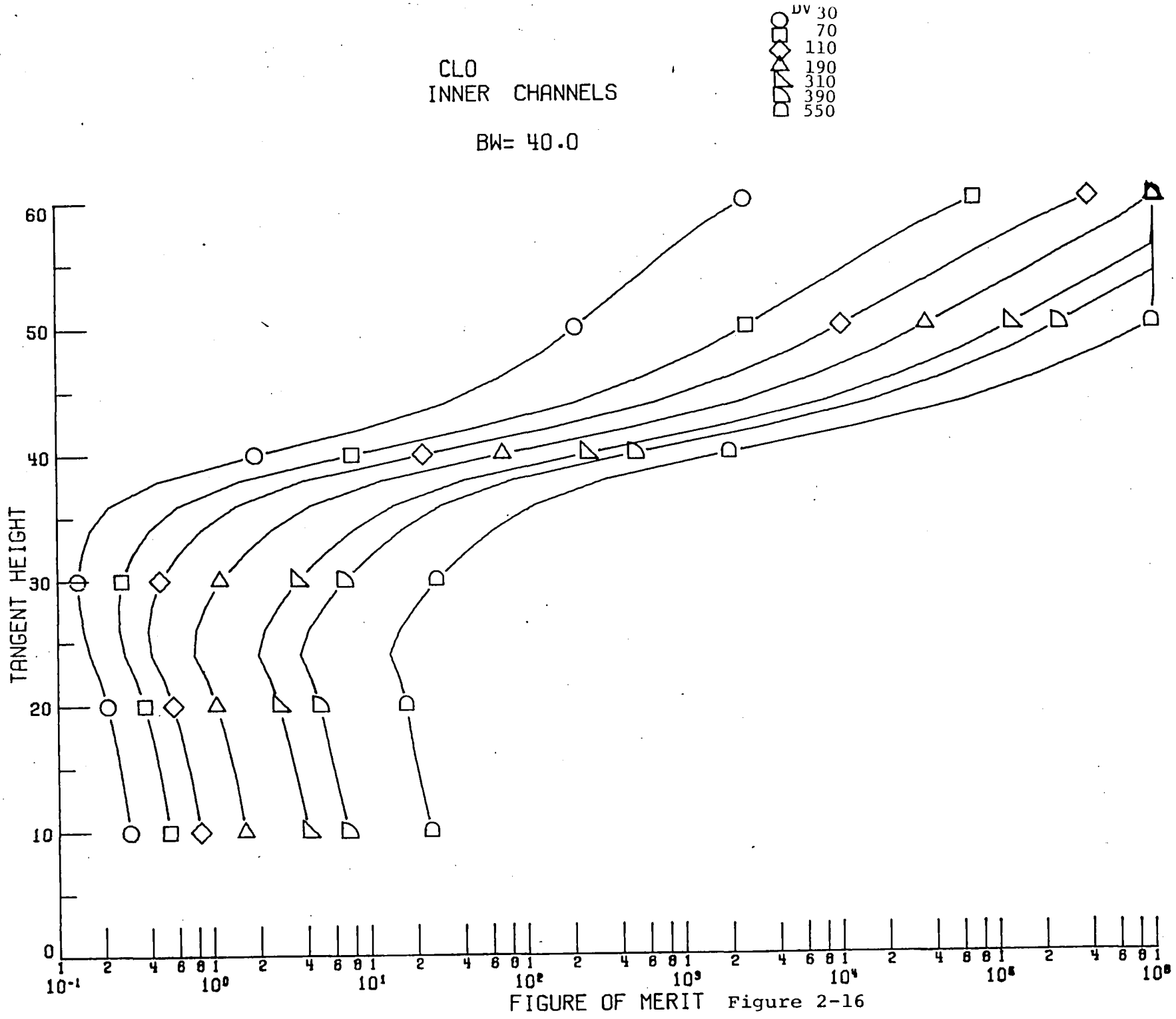
CLO
INNER CHANNELS
BW= 40.0
DV 30
70
110
190
310
390
550
TANGENT HEIGHT
60
50
40
30
20
10
0
1
2
4
6
8
1
10^{-1}
10^{0}
10^{1}
10^{2}
10^{3}
10^{4}
10^{5}
10^{6}
FIGURE OF MERIT

Figure 2-16

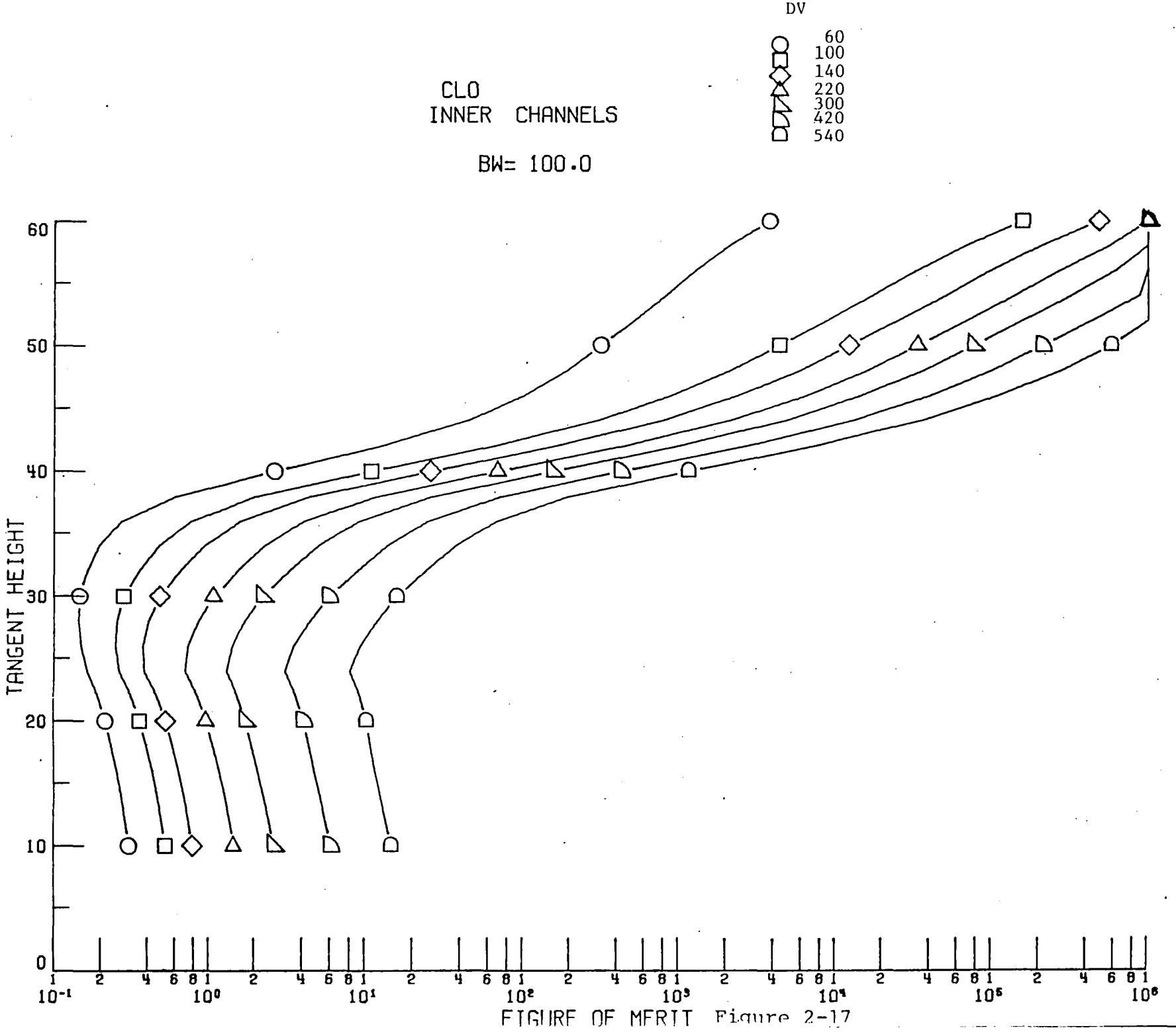
DV
60
100
140
220
300
420
540
CLO
INNER CHANNELS
BW= 100.0
TANGENT HEIGHT
60
50
40
30
20
10
0
1
2
4
6
8
1
2
4
6
8
1
2
4
6
8
1
2
4
6
8
1
2
4
6
8
1
2
4
6
8
1
2
4
6
8
1
10^{-1}
10^{0}
10^{1}
10^{2}
10^{3}
10^{4}
10^{5}
10^{6}
FIGURE OF MERIT
Figure 2-17

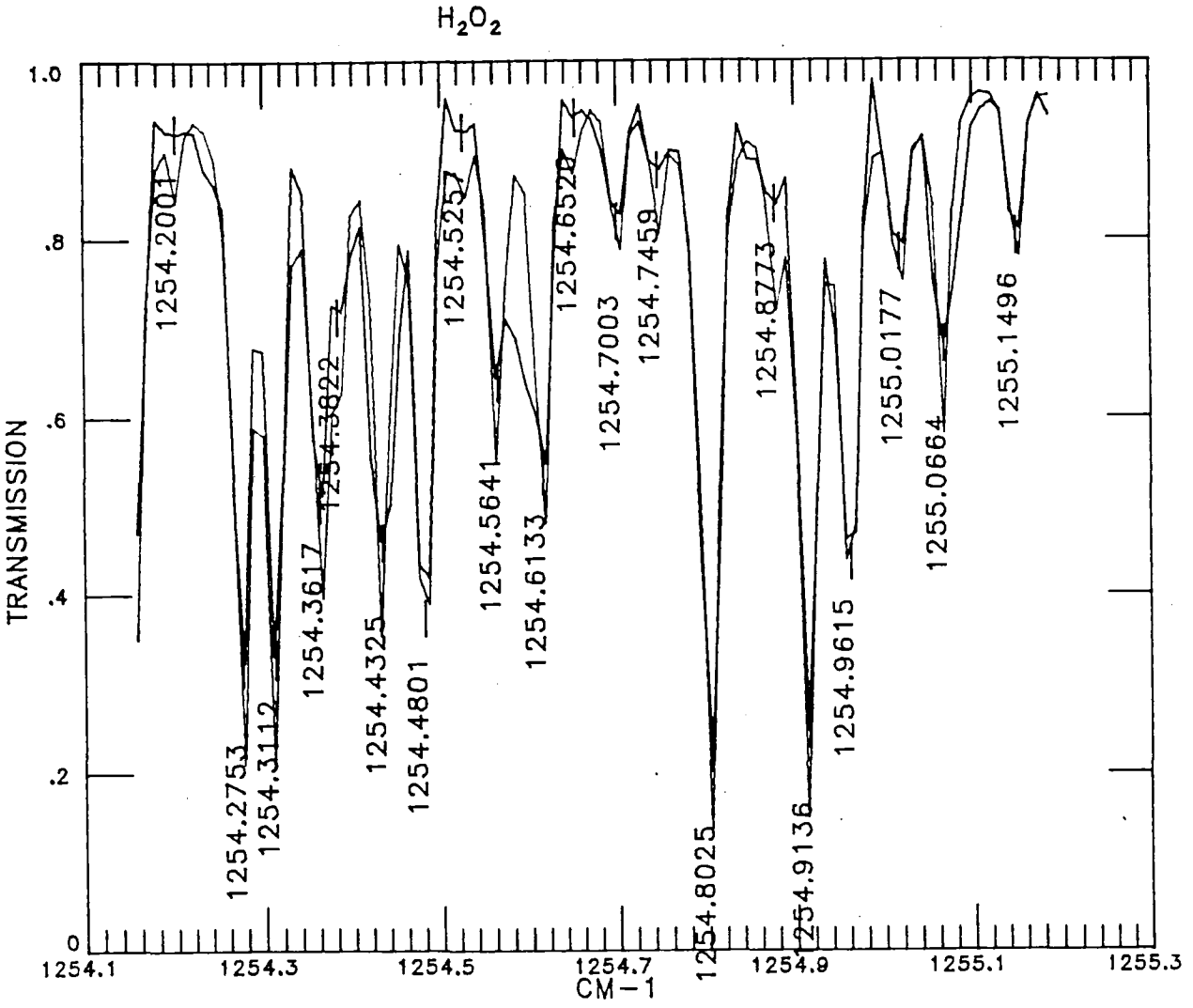
H_2O_2
TRANSMISSION
1.0
.8
.6
.4
.2
0
1254.1
1254.3
1254.5
1254.7
1254.9
1255.1
1255.3
CM-1
1254.2001
1254.2753
1254.3112
1254.3617
1254.3822
1254.4325
1254.4801
1254.5257
1254.5641
1254.6133
1254.6528
1254.7003
1254.7459
1254.8025
1254.8773
1254.9136
1254.9615
1255.0177
1255.0664
1255.1496

Figure 3-1

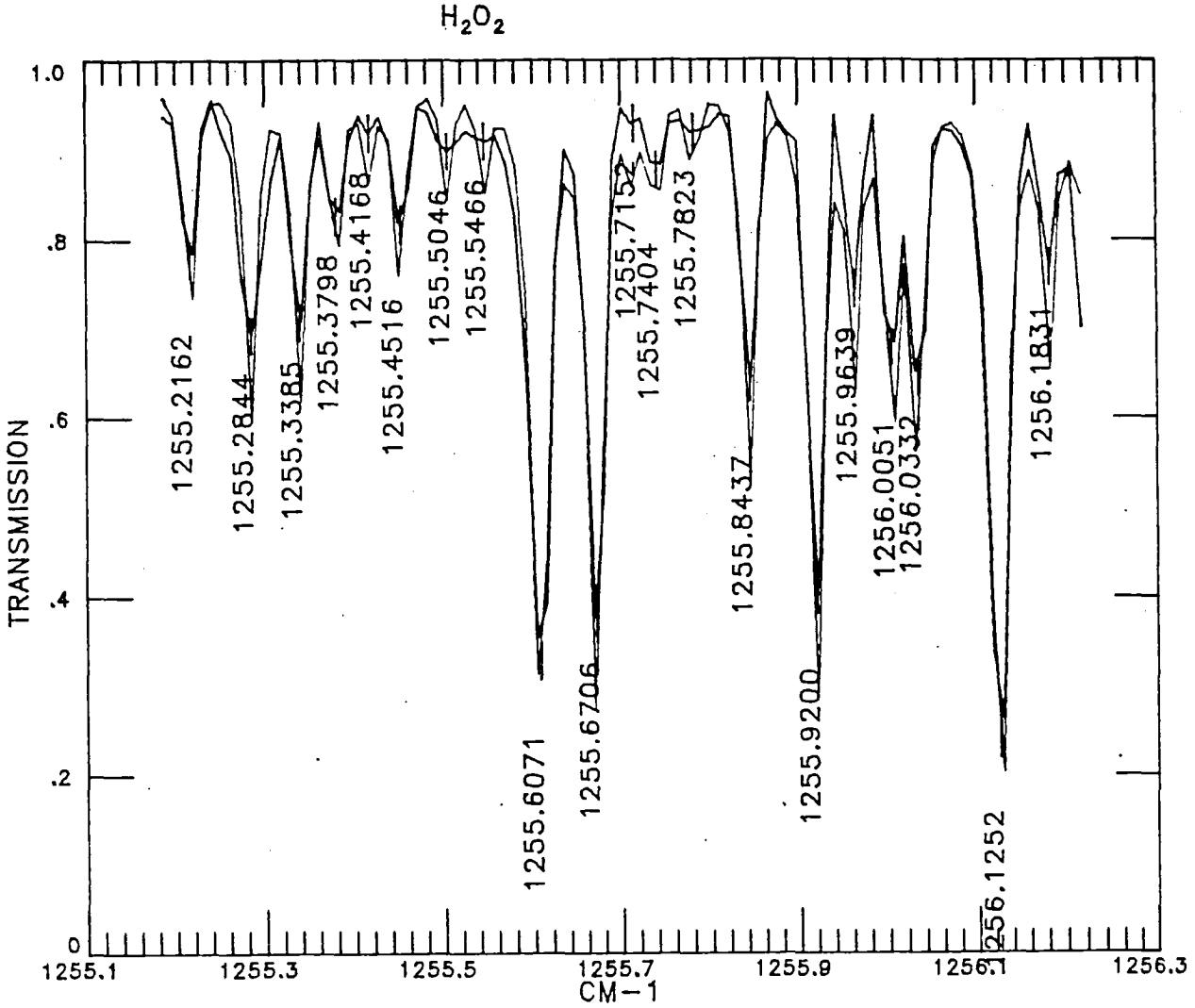
H_2O_2
TRANSMISSION
1.0
.8
.6
.4
.2
0
1255.1
1255.3
1255.5
1255.7
1255.9
1256.1
1256.3
CM-1
1255.2162
1255.2844
1255.3385
1255.3798
1255.4168
1255.4516
1255.5046
1255.5466
1255.6071
1255.6706
1255.7152
1255.7404
1255.7823
1255.8437
1255.9200
1255.9639
1256.0051
1256.0332
1256.1252
1256.1831

Figure 3-2

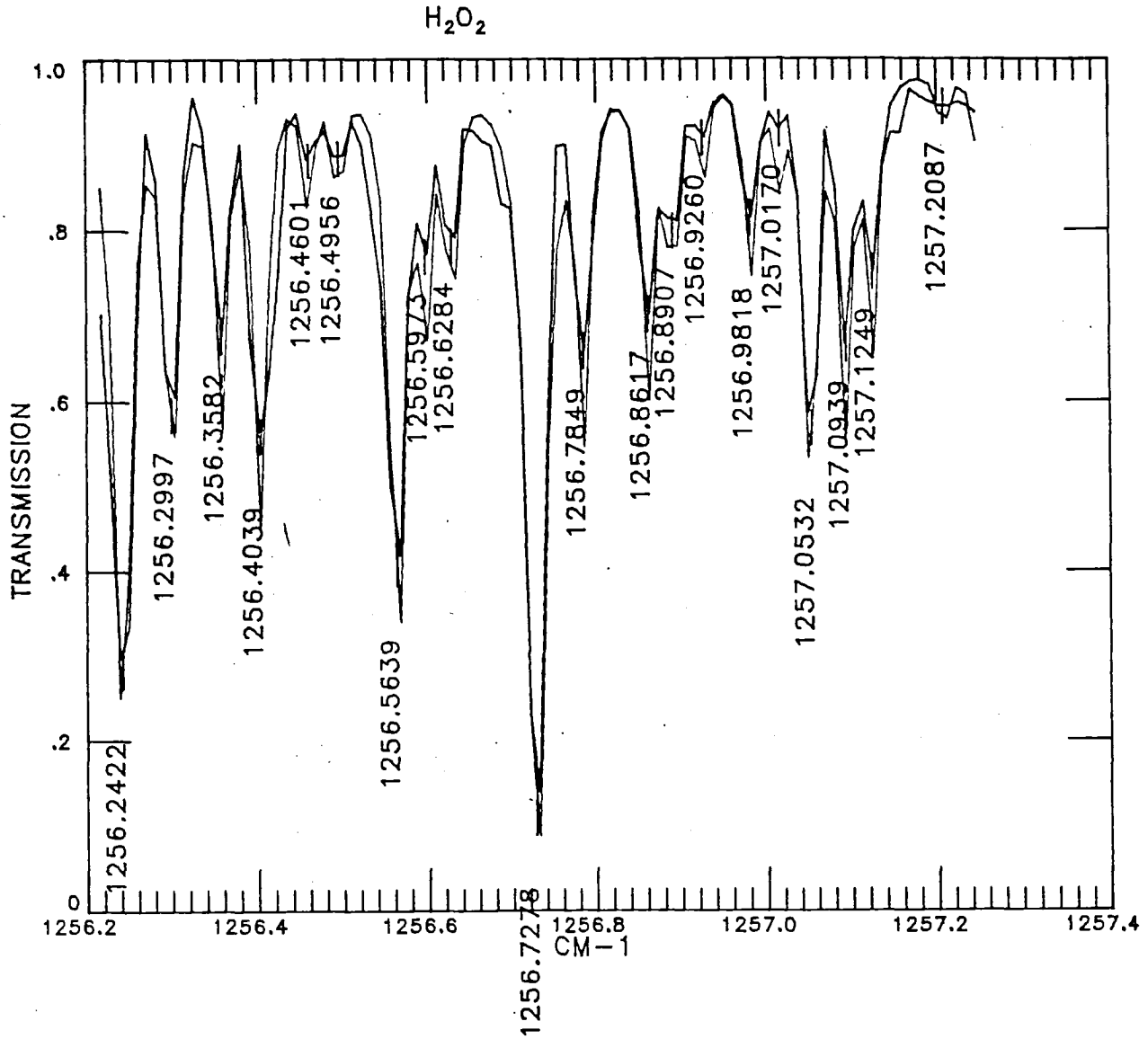
H_2O_2
TRANSMISSION
1.0
.8
.6
.4
.2
0
1256.2
1256.4
1256.6
1256.8
1257.0
1257.2
1257.4
CM-1
1256.2422
1256.2997
1256.3582
1256.4039
1256.4601
1256.4956
1256.5639
1256.5973
1256.6284
1256.7278
1256.7849
1256.8617
1256.8907
1256.9260
1256.9818
1257.0170
1257.0532
1257.0939
1257.1249
1257.2087

Figure 3-3

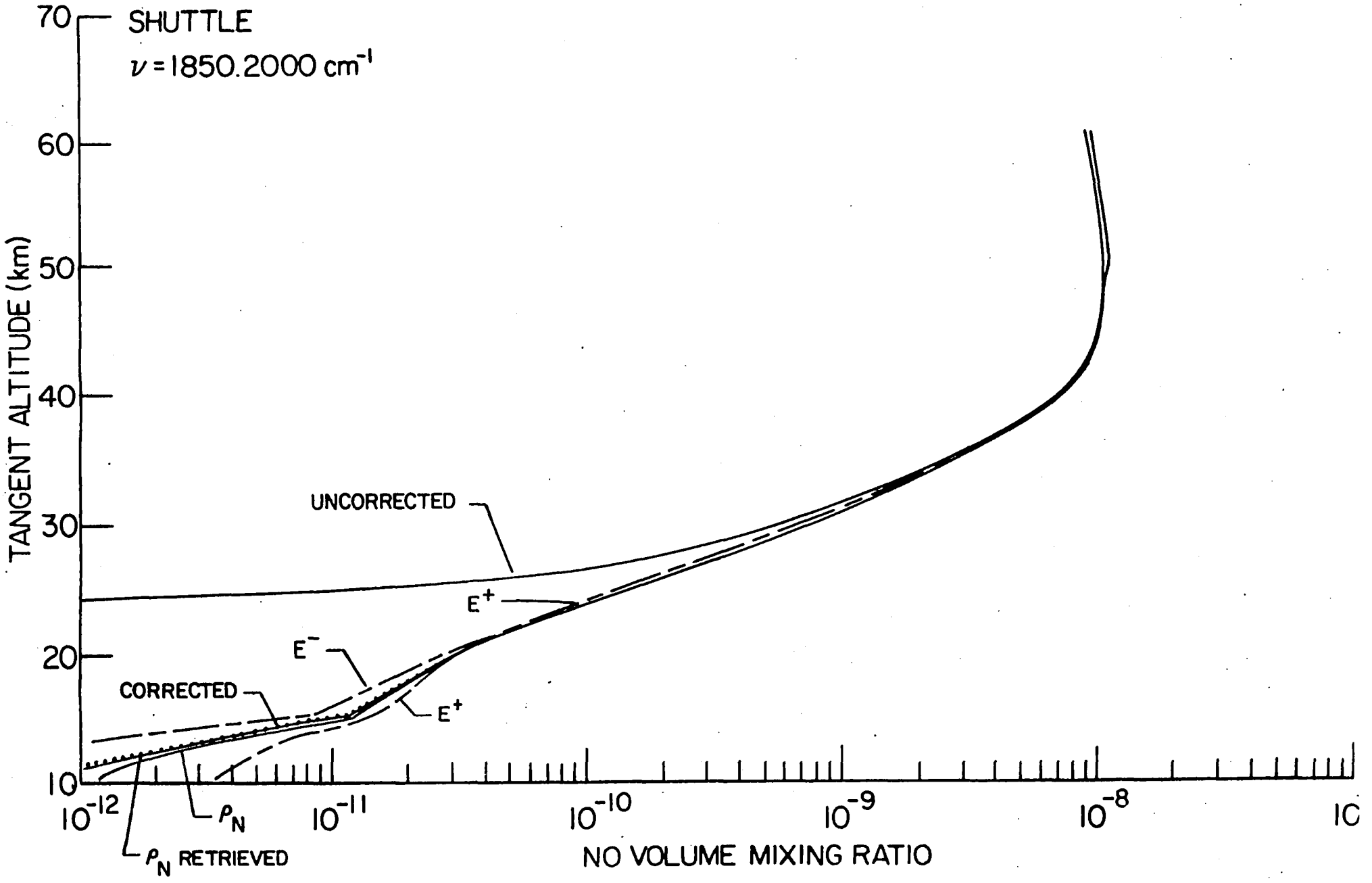
SHUTTLE
ν = 1850.2000 cm^{-1}
TANGENT ALTITUDE (km)
70
60
50
40
30
20
10
UNCORRECTED
E^+
E^-
CORRECTED
E^+
10^{-12}
ρ_N
10^{-11}
10^{-10}
10^{-9}
10^{-8}
IC
ρ_N RETRIEVED
NO VOLUME MIXING RATIO

Figure 4-1

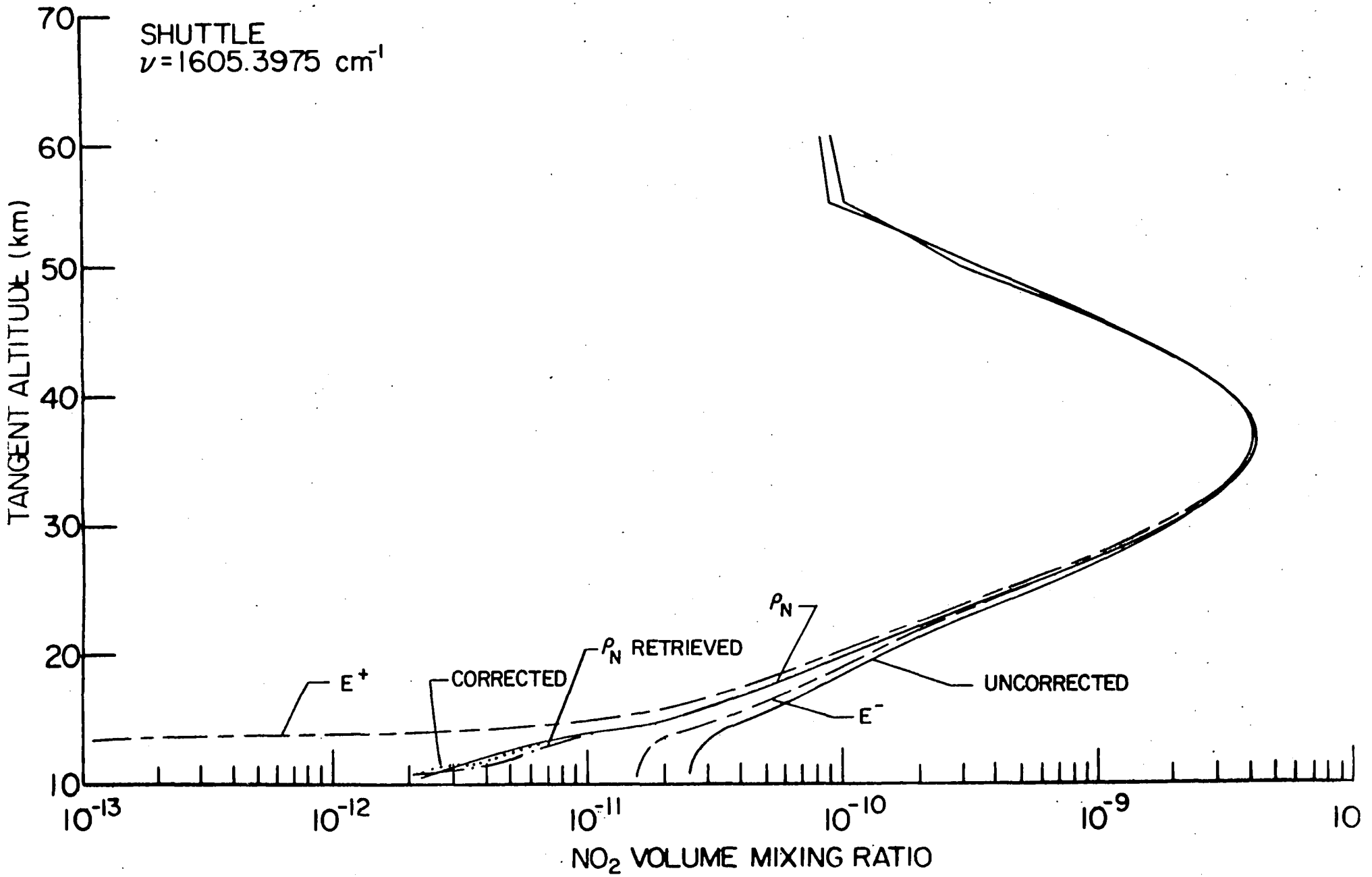
SHUTTLE
ν = 1605.3975 cm⁻¹
TANGENT ALTITUDE (km)
70
60
50
40
30
20
10
10⁻¹³
10⁻¹²
10⁻¹¹
10⁻¹⁰
10⁻⁹
10
NO₂ VOLUME MIXING RATIO
E⁺
CORRECTED
ρN RETRIEVED
ρN
E⁻
UNCORRECTED

Figure 4-2

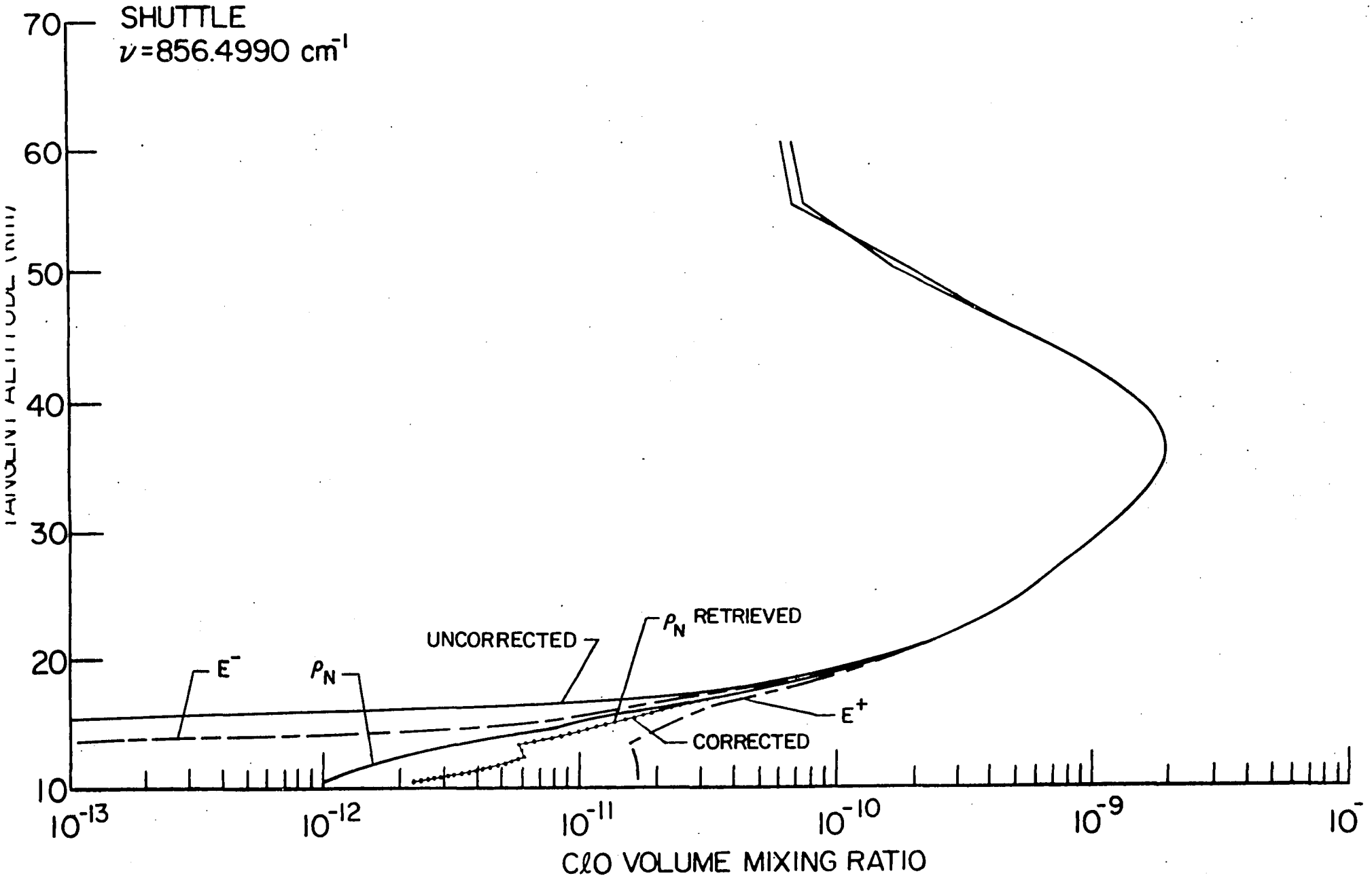
SHUTTLE
ν=856.4990 cm⁻¹
70
60
50
40
30
20
10
TANGENT ALTITUDE (KM)
E⁻
ρN
UNCORRECTED
ρN RETRIEVED
E⁺
CORRECTED
10⁻¹³
10⁻¹²
10⁻¹¹
10⁻¹⁰
10⁻⁹
ClO VOLUME MIXING RATIO

Figure 4-3

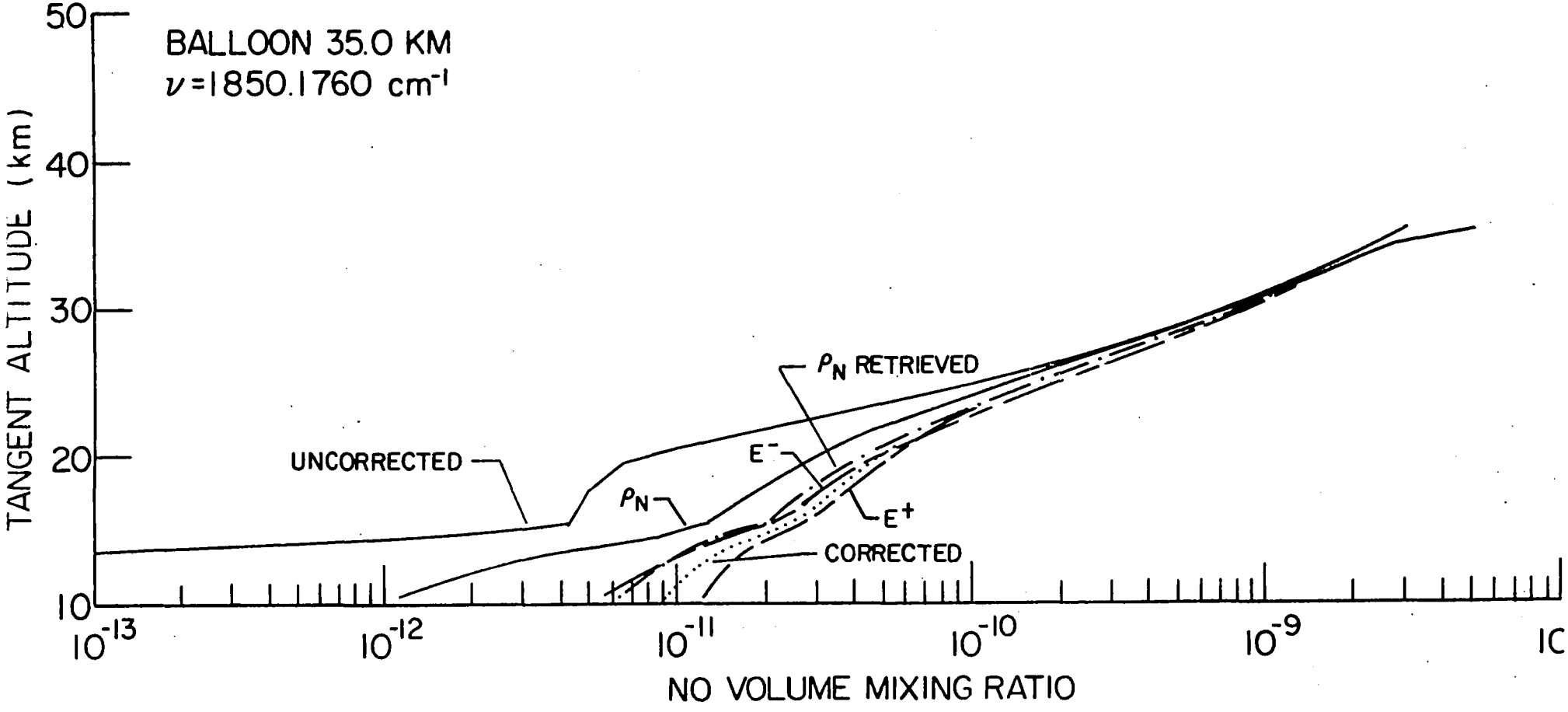
BALLOON 35.0 KM
ν=1850.1760 cm⁻¹
TANGENT ALTITUDE (km)
50
40
30
20
10
ρ_N RETRIEVED
UNCORRECTED
E^-
ρ_N
E^+
CORRECTED
10^{-13}
10^{-12}
10^{-11}
10^{-10}
10^{-9}
IC
NO VOLUME MIXING RATIO

Figure 4-4

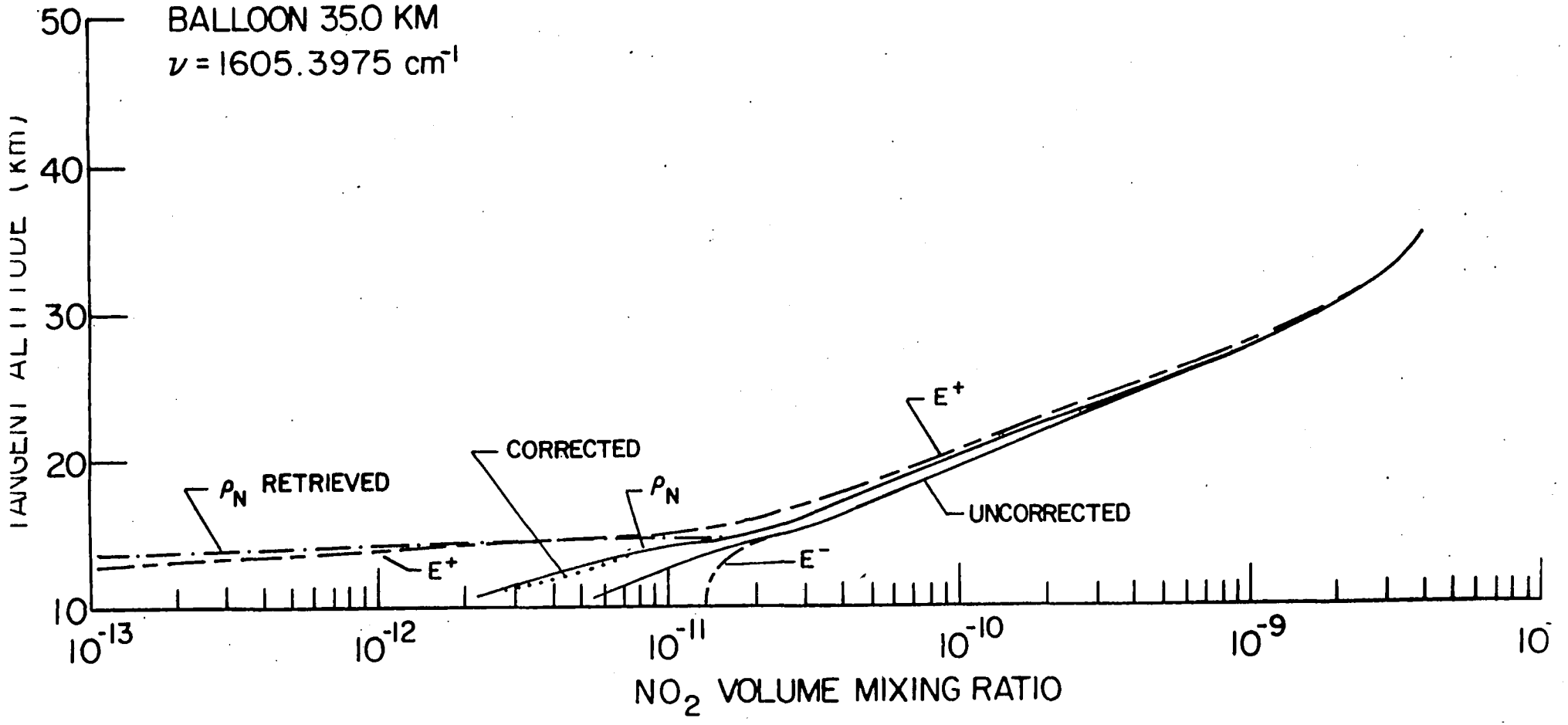
BALLOON 35.0 KM
ν = 1605.3975 cm^{-1}
TANGENT ALTITUDE (KM)
50
40
30
20
10
ρ_N RETRIEVED
CORRECTED
ρ_N
E^+
E^+
E^-
UNCORRECTED
10^{-13}
10^{-12}
10^{-11}
10^{-10}
10^{-9}
NO_2 VOLUME MIXING RATIO

Figure 4-5

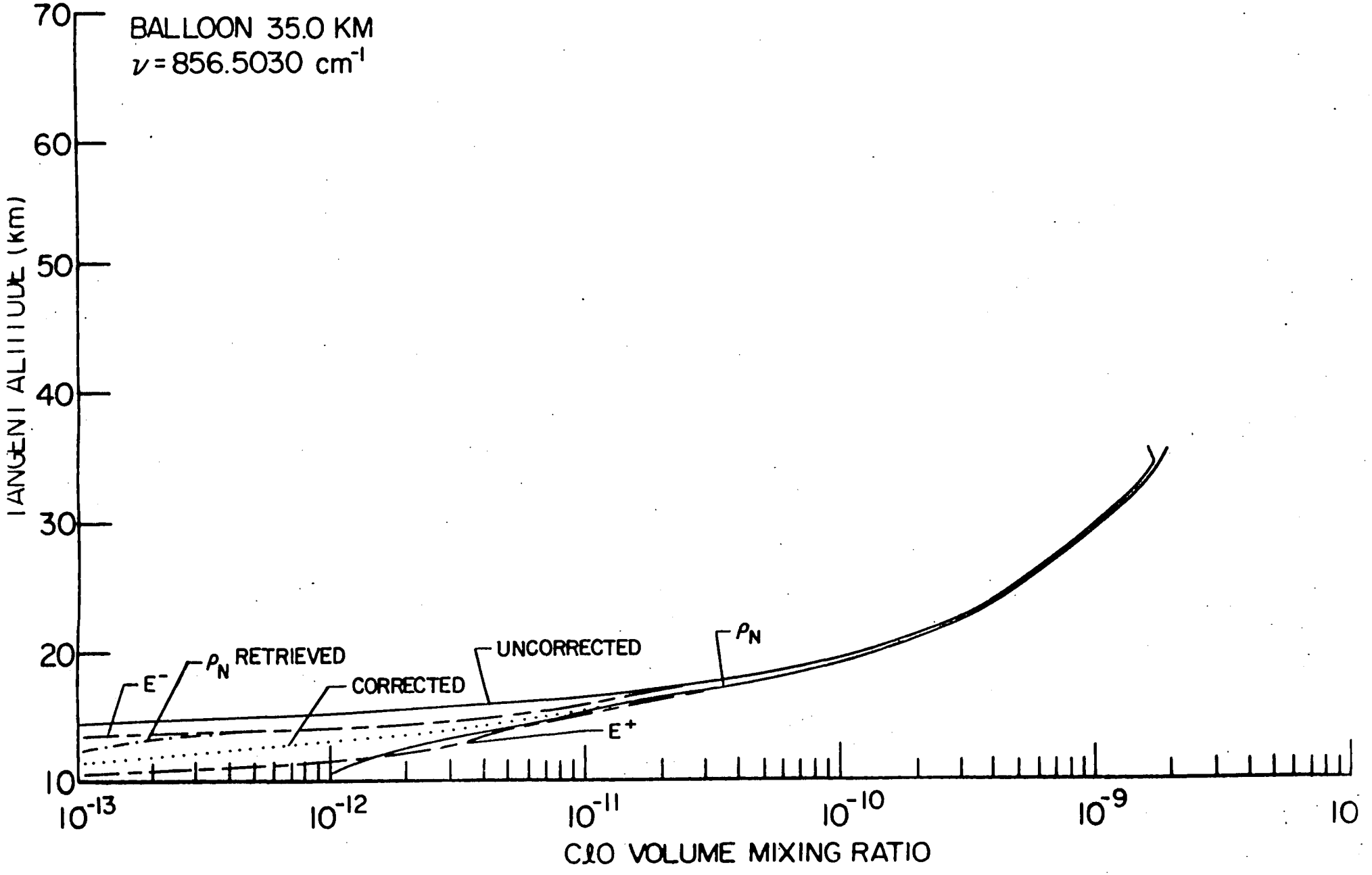
BALLOON 35.0 KM
ν = 856.5030 cm^{-1}
TANGENTIAL ALTITUDE (km)
70
60
50
40
30
20
10
ρ_N RETRIEVED
E^-
CORRECTED
UNCORRECTED
ρ_N
E^+
10^{-13}
10^{-12}
10^{-11}
10^{-10}
10^{-9}
10
ClO VOLUME MIXING RATIO

Figure 4-6

APPENDIX A

INSTRUMENT MODEL

The laser heterodyne spectrometer (LHS) concept is illustrated in Fig. A-1 and a block diagram of the instrument model is shown in Fig. A-2. The front-end of the LHS instrument consists of a conventional optical heterodyne receiver. Solar radiation attenuated by a molecular absorption line of the target gas, combined with the radiation from the tunable diode laser (TDL) local oscillator, is directed onto the Mercury-Cadmium-Telluride photomixer such that the phase fronts are matched as closely as possible to preserve mixing efficiency. Integration over the field of view is accomplished with Siegman's (20) antenna theorem which relates the photomixer area (A) and field of view solid angle (Ω) to the local oscillator wavelength (λ) by

$$\Omega A = \lambda^2$$

The integral of the radiation received at the front of the instrument $N(\nu,H_t)$, over the field of view becomes,

$$N(\nu,H_t) = T(\nu,H_t)\ N_s(\nu)$$

$$P(\nu,H_t) = \int_A \int_\Omega N(\nu,H_t)\ d\Omega da \approx N(\nu,H_t)\ \Omega A = N(\nu,H_t)\lambda^2 \qquad \text{(A-1)}$$

$N_s(\nu)$ - radiance of the sun

$P(\nu,H_t)$ - monochromatic power integrated over detector area and field of view

$T(\nu,H_t)$ - monochromatic transmittance

Monochromatic transmittances, $T(\nu,H_t)$, are calculated from Beers Law using the standard equations for molecular absorption. Transmission losses for the solar radiation signal along the optical path to the photomixer include a 50% loss due to the beam splitter, a 50% loss caused by polarization mismatch between the solar radiation and LO radiation, a 50% loss from lchopping, and a 15% loss due to the optical elements along this path and reflection losses from the photomixer. The TDL is assumed to emit a total 700 uW of power with 80% in a single mode. Because amplitude fluctuations of the dominant mode increase when it is optically isolated from the other weaker modes the instrument has been designed without a mode rejection mechanism. This aspect has been included in the instrument model by calculating the shot noise component based on the total emitted power while the heterodyne signal uses only that power found in the dominant mode. Radiation from the TDL will also experience a 50% loss at the beam splitter, an overfill loss of 10% at the photomixer and a 15% loss due to optical elements and reflection losses at the surface of the photomixer. The heterodyne signal, formed by the product of solar signal and LO radiation, will suffer a mixing loss of 16% caused by phase front mismatch. The output of the photomixer is proportional to the square of the radiation incident upon it, producing a D.C. current proportional to the sum of the incident solar and LO powers and an intermediate frequency alternating current whose amplitude is modulated by the change in solar signal during the scan through

the atmosphere. The heterodyne signal has a spectral signature at intermediate frequencies (I.F.) formed from contributions in the solar spectrum at $\nu_{LO}+\nu_{IF}$ (upper sideband) and $\nu_{LO}-\nu_{IF}$ (lower sideband). A high gain amplifier following the photomixer boosts the heterodyne signal so that it may be channelized with a set of radio frequency filters covering the intermediate frequency range. The channelized signals are now representative of the degree of attenuation that has occurred in each portion of the molecular absorption line. The remainder of the instrument consists of a square law RF detector followed by a low pass filter. The output of the low pass filter is sampled and digitized with a ± 1% uncertainty. The current signal is now proportional to the attenuated solar power and it is this signal which is input to the retrieval algorithm.

Noise sources present in the electrical portion of the receiver include shot noise in the photomixer from the signal and local oscillator, dark current and Johnson noise. Noise sources following the photomixer are expressed as an equivalent noise located at the output of the photomixer and combined with the Johnson noise of the photomixer. The photomixer does not respond uniformly at all intermediate frequencies, with efficiency in general decreasing as one moves to higher intermediate frequencies. The photomixer rolloff used in the model is based on laboratory measurements of a research photomixer from 0 to 500 MHZ which has a D.C. quantum efficiency of 74% and an effective quantum efficiency of 34% at approximately 500 MHZ. Beyond 500 MHZ the effective quantum efficiency was set to 30% in the

instrument model.

In addition to the predicted current signal $I_i(H_t)$ the model also provides an estimate of the expected RMS noise current $IN_i(H_t)$ as a function of tangent height. Together they can be used to calculate the expected signal to noise ratio $I_i(H_t)/IN_i(H_t)$ for the i'th channel. The low pass integration time is chosen to filter out much of the high frequency noise yet still allow the measurement of low frequency components of the signal caused by spatial variations in the concentration profile. The majority of the change in the signal to noise ratio is attributable to the signal change with a small additional effect due to the change in the instrument noise $IN_i(H_t)$ which depends slightly on the input signal.

APPENDIX B

RETRIEVAL ALGORITHMS

The retrieval algorithm uses the "onion-peeling" technique (16-19) to convert the predicted current signal $I_i(H_t)$ to gas concentrations. For a space based platform the procedure starts by ratioing all $I_i(H_t)$ to $I_i(EXO)$, the exoatmospheric current signal ($T(\nu,EXO) = 1$).

$$\frac{I_i(H_t)}{I_i(EXO)} \alpha \frac{P_i(H_t)}{P_i(EXO)} \alpha \frac{\int_{B_{IF}} T(\nu,H_t)G(\nu)N_s(\nu)d\nu}{\int_{B_{IF}} N_s(\nu)G(\nu)d\nu} = \bar{T}_i(\nu,H_t) \quad (A-2)$$

$P_i(H_t)$ is the power in the i'th channel and $\bar{T}(\nu,H_t)$ is a mean transmittance weighted by the instrument frequency response $G(\nu)$ and solar radiance $N_s(\nu)$. This ratio will remove bias differences between channels in the post-channelization portions of the electrical circuit. Note that we have also allowed $N_s(\nu)$ to drop out of equation A-2. This is true only if the instrument field of view remains fixed at the same point on the sun. Relaxing this requirement means an additional factor will appear on the right hand side of equation A-2. The extra factor will be tangent altitude dependent and may be removed by a second ratio between channels which will be discussed in the following paragraph.

In principle, each transmittance profile contains enough information to derive a concentration profile through the entire atmosphere providing the channel is not totally opaque, such as

may occur near line center of a strongly absorbing line over a long absorption path, or conversely that measurable absorption has occurred, which may not be true in the wings of a weak line over a short absorption path. A direct absorption "onion-peel" retrieval could be constructed whereby the concentration at the tangent height would be adjusted until the calculated transmittance matched the measured transmittance to within the instrument error. The final concentration would be ascribed to the tangent height and become available for use in the transmittance calculations at all lower measurement tangent heights. In this way the number of unknown concentrations along the absorption path is reduced to only the concentration at the tangent height. The direct absorption technique, while simple and straight forward, can be subject to significant errors caused by background absorption continuum and the wings of lines located beyond the instrument passband. Some of these effects can of course be removed provided the cause of the absorption is known and can be correctly modeled for inclusion in the transmittance calculations. This correction procedure can be avoided entirely when the interfering absorption has a small spectral variation over the instrument passband by forming a second ratio between channels at the same tangent altitude.

$$TR(H_t) = \frac{\bar{T}_i(H_t)}{T_j(H_t)} \qquad \text{(A-3)}$$

$TR(H_t)$ is representative of the differential absorption between

channels i and j. For a LO tuned to the center of a single absorption line the j'th channel will generally cover the wings while the i'th channel will lie between it and line center. It is not necessary that the j'th channel be totally clear for the technique to work, only that some differential absorption exist between the channels. A disadvantage of the differential absorption technique as compared to the direct absorption method involves the noise level of the quantity being matched in the iterative process. The direct absorption method matches transmittance with its attendant instrument error while the differential absorption technique uses the ratio of two transmittances both containing instrument errors and the error in the transmittance ratio (TR) will be the square root of the sum of the squares of the individual errors present in each channel. The increased noise level is not that severe a penalty to pay when working with a weakly absorbing gas such as HNO_3 or H_2O_2. Channel five (closest to line center) would be the likely channel to use in the direct absorption technique and including channel one (in the line wings) to form $TR(H_t)$ in the differential absorption technique will raise the noise level in $TR(H_t)$ only slightly above that of $T_5(H_t)$ since the signal to noise ratio of channel one is much greater than that of channel five. For O_3 there are some channel combinations where this is not true and the overall noise level of TR will be greater than a single channel.

In the evaluation of equation A-3 several different combinations of two channels may be formed from the five channels

of information available at a particular tangent altitude. One of these combinations will be superior to the others in its ability to minimize the random errors in the retrieved concentrations. One would intuitively expect the quality of one channel combination relative to another combination to depend not only on the signal to noise ratios of the channels used in the ratio but also upon the amount of differential absorption a pair of channels will produce. This is indeed the case. An expression may be developed relating the relative error in the retrieved concentration at a particular tangent altitude to the uncertainty present in the transmission ratio TR. The pair of channels that minimizes the expression,

$$\frac{\varepsilon}{|\ell n(TR(H_t))|} \quad \begin{matrix} \alpha \\ \text{Concentration Relative Errors} \end{matrix} \qquad \begin{matrix} \text{Tangent Height} \\ \\ \end{matrix} \tag{A-4}$$

$$\varepsilon = \left[\left(\frac{1}{SNR_i}\right)^2 + \left(\frac{1}{SNR_j}\right)^2\right]^{\frac{1}{2}}$$

will produce the least error in the inferred concentration. SNR_i in the equations above represents the signal to noise ratio of the i'th channel.

After the optimum pair of channels have been chosen for each measurement altitude the "onion-peel" process can begin at the top of the atmosphere. The process begins at the altitude where enough absorption has occurred to produce a signal change greater than the random instrument noise. At this point a mean concentration covering the shell between the current tangent height and next highest tangent height is iterated until the

calculated transmittance ratio matches the measured transmittance ratio to within the expected instrument noise. The convergence criteria may be expressed as,

$$E = \frac{TR^m(H_t) - TR^c(H_t)}{TR^m(H_t)} \qquad \text{(A-5)}$$

where the superscript c signifies quantities calculated in the retrieval process and the superscript m identifies quantities derived from measurements. The Newton-Raphson process is used to adjust the mean concentration until convergence occurs. This technique requires two initial concentrations before a third can be predicted. At the start of the onion-peel process the first concentration is set to a value four orders of magnitude smaller than the maximum expected value. Once inside the atmosphere the first concentration is set equal to the concentration at the previous level. For both situations the second concentration is selected to be 10% larger than the first value. Transmittance, transmittance ratios, and finally the errors E are calculated using both of the initial concentration values. At this point a third concentration is predicted followed by a calculation of it's error. The concentration corresponding to the largest error E is thrown out and a new prediction is made. This process continues until the convergence criteria is satisfied. In general convergence occurs rapidly, usually within 2 to 3 iterations. The same procedure is applied at the next lower measurement tangent height except that now the previous concentration is used

in the transmittance calculation and assumed fixed while the mean concentration of the shell above the measurement altitude is adjusted until convergence occurs. Continuing the process to an expected lower limit of 10 km due to clouds generates a profile over a region where measureable differential absorption has occurred. This formulation of the "onion-peel" retrieval is extremely stable. Artificial introduction of a concentration error of ± 20% from the iterated solution causes errors in the retrieved concentrations below this point that damps out in two to three measurement levels. One drawback of the "onion-peel" technique is its implicit assumption of spherical symmetry. Some photochemically active trace gases undergo large diurnal variations with rapid concentration changes occurring at sunrise or sunset which can produce large errors when this type of retrieval technique is used (1,14).

The retrieval errors are typically larger above and below the concentration peak of the target gas. Above the peak little absorption occurs and one is faced with the problem of inferring a concentration from an optical depth containing uncertainties sometimes as large as the optical depth itself. Below the peak the optical depth decreases again in the tangent height shell while the majority of the absorption occurs at higher altitudes. Since the majority of the absorption is known (from calculations at the previous tangent altitudes) one is again inferring a concentration at the tangent height from an optical depth containing a large uncertainty.

Concentration retrievals from a balloon platform are

performed in essentially the same manner as from a space platform. One must account for the reduced absorption path length due to the measurement geometry. In general, for a high altitude balloon (35 to 40 km), and for gases with concentration peaks below the float altitude, this reduction is small and the accuracy of the retrieval is only slightly less than that achievable from a space platform. The other major change required for the balloon retrieval is modification of the retrieval algorithm to account for the absorber amount above the balloon float altitude. To a first approximation the absorber amount above the balloon may be modeled with either an average concentration or average mixing ratio depending on which quantity has the best vertical variation. The average concentration or mixing ratio can be calculated from hi-sun data (solar zenith angle $< 90^{o}$) with the same iterative process used at the lower levels. If hi-sun data is not available the retrieved average concentration or mixing ratio will represent the average from the tangent altitude corresponding to this first scan up to the top of the atmosphere. At lower tangent altitudes the onion-peel process proceeds normally. Since one does not have exoatmospheric data as required by equation A-2 to calculate an absolute averaged channel transmittance, additional pre or post-flight calibration work must be performed. Heterodyning against a black body will give the relative channel to channel response which may be incorporated into equation A-3 to again define a transmittance ratio of two IF channels.

Aircraft or ground based measurements require an entirely

different type of retrieval. From a balloon or space platform vertical profile information may be inferred from changes in the physical geometry as the viewing angle changes during the measurement. The vertical profile information for aircraft or ground based measurements comes from absorption line shape changes caused by collisional broadening. The vertical resolution is typically on the order of 4-5 km and no information on the vertical profile is available above 25 to 30 km. A full description of this retrieval technique may be found in (13).

LASER HETERODYNE SPECTROMETER CONCEPT

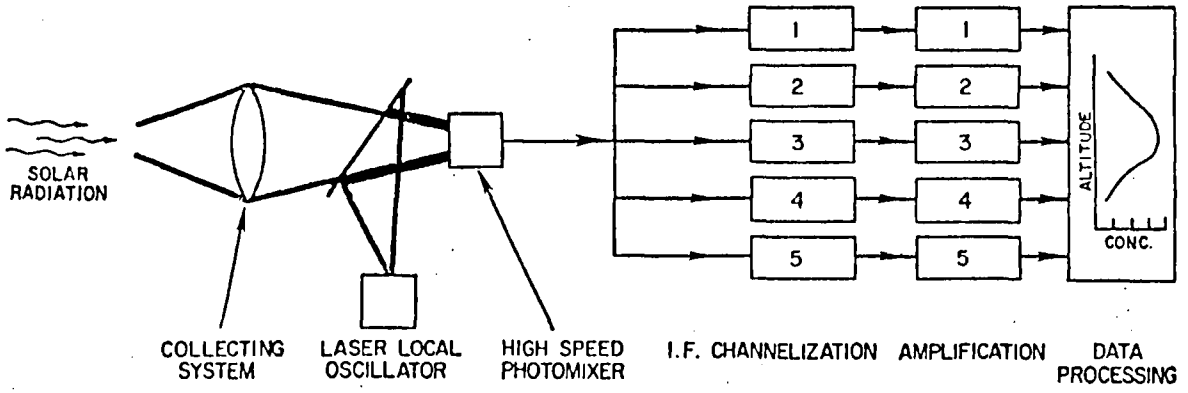

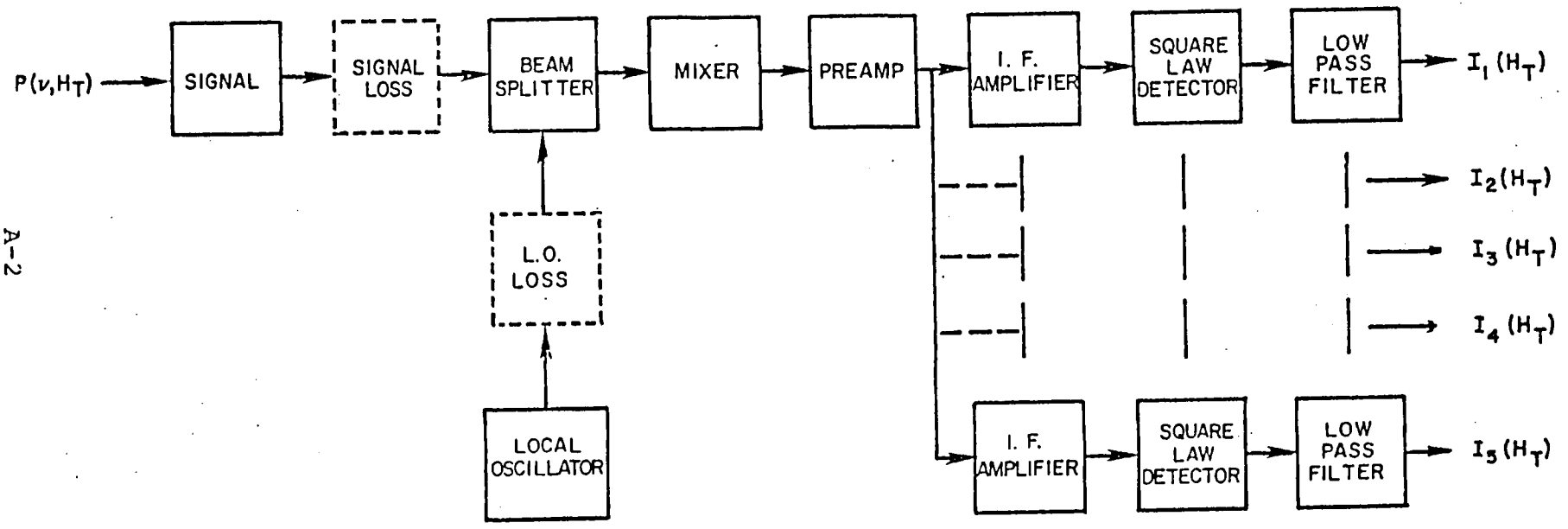
P(ν,H_T)
SIGNAL
SIGNAL LOSS
BEAM SPLITTER
MIXER
PREAMP
I. F. AMPLIFIER
SQUARE LAW DETECTOR
LOW PASS FILTER
I_1(H_T)
I_2(H_T)
I_3(H_T)
I_4(H_T)
L.O. LOSS
LOCAL OSCILLATOR
I. F. AMPLIFIER
SQUARE LAW DETECTOR
LOW PASS FILTER
I_5(H_T)

1. Report No.	2. Government Accession No.	3. Recipient's Catalog No.
NASA CR-172348		

4. Title and Subtitle	5. Report Date
Advanced Laser Stratospheric Monitoring Systems Analyses	June 29, 1984
	6. Performing Organization Code
7. Author(s)	8. Performing Organization Report No.
Jack C. Larsen	
9. Performing Organization Name and Address	10. Work Unit No.
Systems and Applied Sciences Corporation 17 Research Drive Hampton, VA 23666	11. Contract or Grant No. NAS1-15806
12. Sponsoring Agency Name and Address	13. Type of Report and Period Covered
National Aeronautics and Space Administration Washington, DC 20546	Contractor Report
	14. Sponsoring Agency Code 506-54-23-20

15. Supplementary Notes

Langley Technical Monitor: Jose M. Alvarez
Final Report

16. Abstract

This report describes the software support for the Laser Heterodyne Spectrometer Experiment. This report discusses improvements to the Langley spectroscopic data base, development of LHS instrument control software and data analyses and validation software. The effect of diurnal variations on the retrieved concentration of NO, NO_2 and ClO from a space and balloon borne measurement platform are discussed along with the selection of optimum IF channels for sensing stratospheric species from space.

17. Key Words (Suggested by Author(s))	18. Distribution Statement
Infrared, Onion Peel, Occultation, Heterodyne, Diurnal Variations	Unclassified-Unlimited Subject Category 66

19. Security Classif. (of this report)	20. Security Classif. (of this page)	21. No. of Pages	22. Price
Unclassified	Unclassified	72	

For sale by the National Technical Information Service, Springfield, Virginia 22161